

Quantum correlations and spatial localization in trapped one-dimensional ultra-cold Bose-Bose-Bose mixtures

Tran Duong Anh-Tai,^{1,*} Miguel A. García-March,^{2,†} Thomas Busch,¹ and Thomás Fogarty^{1,‡}

¹*Quantum Systems Unit, OIST Graduate University, Onna, Okinawa 904-0495, Japan*

²*Instituto Universitario de Matemática Pura y Aplicada,
Universitat Politècnica de València, E-46022 València, Spain*

(Dated: January 28, 2025)

We systematically investigate and illustrate the complete ground-state phase diagram for a one-dimensional, three-species mixture of a few repulsively interacting bosons trapped harmonically. To numerically obtain the solutions to the many-body Schrödinger equation, we employ the improved Exact Diagonalization method [T. D. Anh-Tai *et al.*, SciPost Physics 15, 048 (2023)], which is capable of treating strongly-correlated few-body systems from first principles in an efficiently truncated Hilbert space. We present our comprehensive results for all possible combinations of intra- and interspecies interactions in the extreme limits that are either the ideal limit ($g = 0$) or close to the hard-core limit ($g \rightarrow \infty$). These results show the emergence of unique ground-state properties related to correlations, coherence and spatial localization stemming from strongly repulsive interactions.

Keywords: ultra-cold bosonic quantum gases, improved exact diagonalization, strongly-correlated few-body systems

I. INTRODUCTION

Over the past three decades, ultra-cold atomic gases have been an excellent and unique platform to explore the fascinating physics of complex many-body quantum systems in a very clean setting with high degrees of control. Moreover, they possess a great number of promising applications for quantum technologies such as quantum simulators [1–3], and quantum metrology [4]. Although the physics of weakly-interacting ultra-cold bosonic gases is important and well understood within the framework of Gross-Pitaevskii mean-field theory [5, 6], investigating systems of few bosons, fermions, and mixtures thereof in low dimensional space, where correlations are of importance, is an equally important and intriguing area of research [7, 8]. Recent advances in laser cooling techniques and quantum optics have made it feasible to create strongly-correlated systems in low dimensions with well-defined particle numbers in laboratories [9–18], which has stimulated extensive beyond-mean-field studies of few-body one- and two-component systems in parallel to mean-field studies.

When the repulsive interaction strength in a one-dimensional single-species bosonic gas is varied from being weak to being strong, the system undergoes a transition from condensation to fermionization [19, 20]. In the infinitely repulsive limit, the bosonic system can be mapped to a non-interacting, spin-polarized Fermi gas and its wavefunction can be analytically obtained by the Bose-Fermi mapping theorem [21]. This is referred to as the Tonk-Girardeau hard-core limit, which has been experimentally realized [9, 11]. Meanwhile, binary mixtures exhibit additional phenomena due to the presence of the interspecies interaction or different particle statistics. For instance, when the interspecies coupling strengths are large, binary bosonic mixtures can exhibit a phase-separated state [22–26] or form a composite-fermionization phase [27–29] depending on the intraspecies interactions being strong or weak, respectively. Similar phases can appear in binary mixtures of few particles, with the ground-state properties having been fully explored in Ref. [30]. Furthermore, when considering weaker interactions away from the integrable hard-core and ideal BEC limits the system is rather complex and can display strong signatures of quantum chaos due to the abundance of avoided crossings in the energy spectrum [31, 32]. Importantly, binary few-body mixtures have also emerged as an excellent platform for gaining deeper insights into impurity physics [33–38] and few-body quantum droplets [39–42], as correlation effects can be more easily assessed due to access to the full quantum many-body state.

Extending studies to triple-species mixtures, which possess an even larger parameter space compared to single and binary mixtures, is therefore likely to unveil even richer physics and function as a guide to future experiments. Although it is computationally challenging to accurately solve the many-body Schrödinger equation in continuous 1D space due to the large Hilbert space, efficient numerical tools have recently been developed for this purpose such as the multi-layer multi-configuration time-dependent Hartree method for mixtures of identical particles [43–45] or the

* tai.tran@oist.jp

† garciamarch@mat.upv.es

‡ thomas.fogarty@oist.jp

improved Exact Diagonalization method [32]. So far, the studies on three-species few-particle systems have mainly focused on correlations and entanglement between two distinguishable impurities coupled to a quantum few-boson bath [46, 47] and on engineering strongly-correlated atomic Bell states [38]. For a more systematic approach we will in the following explore the ground-state properties, including the correlations, coherence and self-organization, across all possible interaction regimes for a three-species mixture of a few bosons confined in a one-dimensional harmonic trap from first principles.

The main goal of this work is to explore and illustrate the complete ground-state phase diagram of the system when the intra- and interspecies interactions are either in the ideal limit ($g = 0$) or close to the hard-core limit ($g \rightarrow \infty$). For this we use the one-body density distribution function to characterize the spatial localization, the reduced one- and two-body density matrices, and the bipartite mutual information as the indicators for quantum correlations and coherence. As one of the main results, we find that the ground-state phases of the system with respect to all possible combinations of the interaction strengths can be classified into two groups. The first group consists of phases that exhibit correlations in only one or two species and this group is well-studied theoretically in previous works. In the second group all three species are coupled and hence exhibit interesting results which are unique to three-species bosonic mixtures. We therefore focus on the second group and concisely explore the static ground-state properties of all possible combinations of interaction strengths in this group. Additionally, we systematically investigate the correlations and coherence properties for a representative example where two intraspecies coupling strengths vary between the ideal BEC limit and the hard-core limit, thereby connecting two of the limiting phases. We will show that interesting effects can be observed also in the moderate interaction regime. Our numerical approach to the solution of the many-body Schrödinger equation is based on the improved Exact Diagonalization method [32], which grants us access to the correlated ground-state wavefunction of the system, and the above-mentioned quantities of interest with a reasonable computational cost. We remark that our results contribute to the insightful understanding of correlation effects in complex many-body quantum systems due to strong particle-particle interactions and are relevant to future experiments on strongly-correlated multi-species ultra-cold quantum gases.

Our manuscript is organized as follows: Section II introduces the Hamiltonian of our model, the ab initio method employed for the numerical solutions of the many-body Schrödinger equation, and the quantities of interest characterizing quantum correlations, coherence and spatial self-organization. In Section III we present the main findings related to the static ground-state properties of three special tri-correlated phases and one representative connection between extreme states. Section IV presents the conclusions and outlook. Finally, for completeness, we discuss the remaining tri-correlated cases, which can be seen as extensions of smaller systems, in Appendix A.

II. MODEL, METHODOLOGY, AND QUANTITIES OF INTEREST

A. Model

We consider a three-species mixture of repulsively interacting bosonic atoms trapped in a one-dimensional parabolic potential with frequency ω . We assume that each component $\sigma \in \{A, B, C\}$ has a minimal, but well-defined particle number, $N_\sigma = 2$, and that all masses are equal, $m_\sigma = m$. Since we only consider systems at low temperatures, the two-body scattering potential is well captured by a s -wave pseudo-potential that is usually modeled by a δ -function [48]. Hereafter, we use harmonic oscillator units to rescale the many-body Hamiltonian which means that all lengths, energies, and coupling strengths will be given in terms of $\sqrt{\hbar/(m\omega)}$, $\hbar\omega$, and $\sqrt{\hbar^3\omega/m}$, respectively. The dimensionless Hamiltonian describing our system reads

$$\hat{H} = \sum_{\sigma} \hat{H}^{\sigma} + \sum_{\sigma \neq \delta} \hat{W}^{\sigma\delta}, \quad (1)$$

where \hat{H}^{σ} denotes the σ -species Hamiltonian, while $\hat{W}^{\sigma\delta}$ describes the interactions between two species σ and δ . Explicitly they are given as

$$\hat{H}^{\sigma} = \sum_{i=1}^{N_{\sigma}} \left[-\frac{1}{2} \frac{d^2}{d(x_i^{\sigma})^2} + \frac{1}{2} (x_i^{\sigma})^2 + g_{\sigma} \sum_{i < j} \delta(x_i^{\sigma} - x_j^{\sigma}) \right], \quad (2)$$

$$\hat{W}^{\sigma\delta} = g_{\sigma\delta} \sum_{i=1}^{N_{\sigma}} \sum_{j=1}^{N_{\delta}} \delta(x_i^{\sigma} - x_j^{\delta}). \quad (3)$$

Here the terms g_{σ} and $g_{\sigma\delta}$ correspond to the intra- and interspecies coupling strengths respectively, which can be experimentally tuned from the ideal BEC limit ($g = 0$) to the hard-core Tonks-Girardeau (TG) limit ($g \rightarrow \infty$) by using

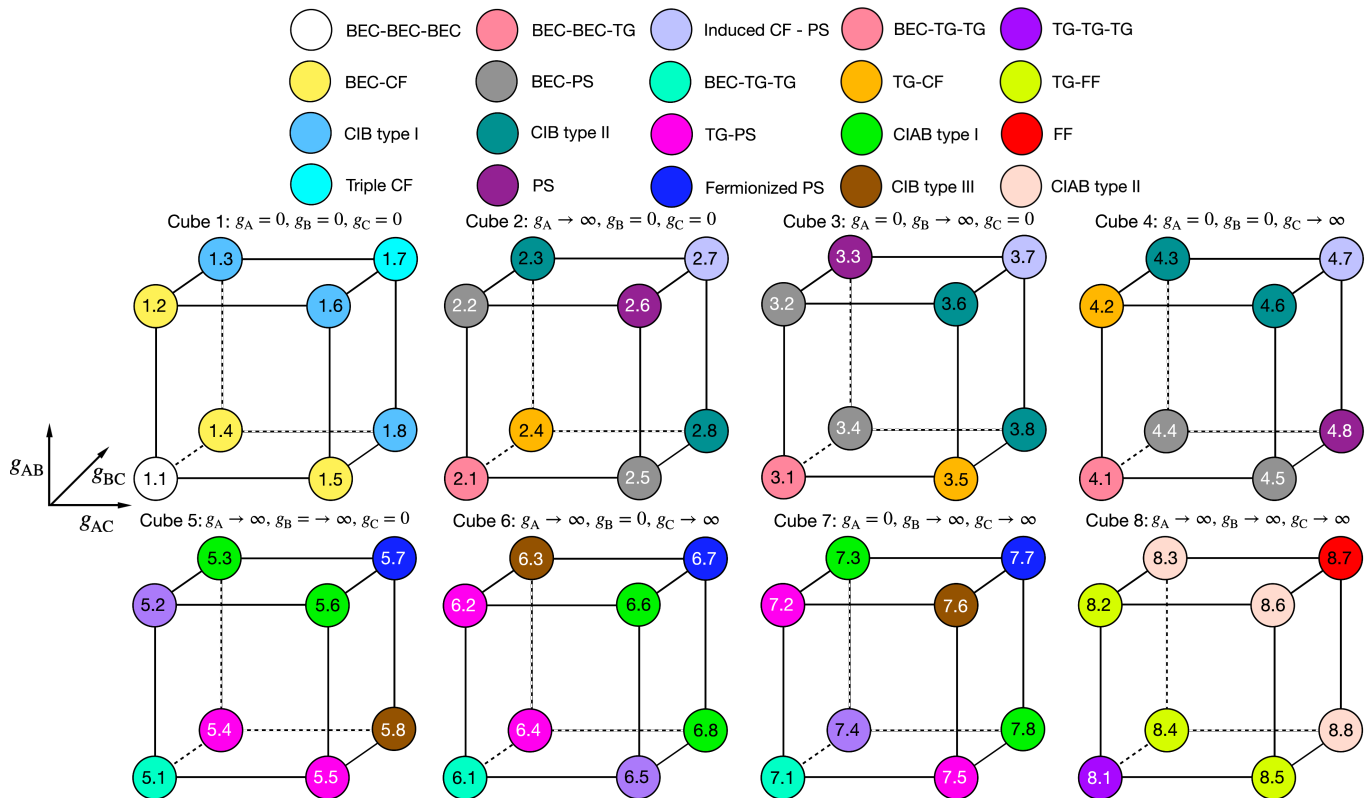


FIG. 1. The complete ground-state phase diagram of a three-species mixture of a few repulsively interacting bosons confined in a one-dimensional harmonic trap. Each cube corresponds to a set of intraspecies interaction strengths $\{g_A, g_B, g_C\}$ (given in the title of each cube) while the interspecies interaction strengths $\{g_{AB}, g_{AC}, g_{BC}\}$ increase along the edges with $(0, 0, 0)$ corresponding to the lower left corner. All corners are numbered to be easily identifiable in Table I, and the corners with the same color correspond to the same phase.

Feshbach [49] or confinement-induced resonances [50]. It is noted that as the numerical calculations cannot account for $g = \infty$, we use the coupling strength $g = 20$ to describe the hard-core TG limit throughout this work. This has been shown in previous works to give results that are sufficiently close to infinite interactions [26, 27, 29, 30, 32].

Given that we consider a three-species mixture with elastic two-body collisions only, the system is described by six coupling strengths that explicitly are $g_A, g_B, g_C, g_{AB}, g_{AC}$, and g_{BC} , and since we are only interested in the limits when these strengths are either $g = 0$ or $g \rightarrow \infty$, all possible combinations of the six coupling strengths result in a total of 64 cases to be considered and the complete phase diagram of the system can be schematically represented by the eight cubes shown in Fig. 1. However, due to the assumption of equal masses and particle numbers in each species these reduce to 32 distinct ones, and we also note that some of the distinct states can be straightforwardly understood from the known solutions of the single components and the binary mixtures, whenever one or two components decouple (see the left sub-table in Table I). In particular, in the absence of all interspecies interactions, $g_{AB} = g_{AC} = g_{BC} = 0$, the many-body Hamiltonian (1) factorises, and the exact solutions can be found in the ideal limit, as well as in the TG limit via the Bose-Fermi mapping theorem [21, 51]. The resulting states therefore lack any interspecies correlations and are simply uncorrelated combinations of BEC and TG gases (see the first four phases listed in the left sub-table in Table I). In the situation in which only one interspecies interaction tends to infinity, the system can be decoupled into two separated subsystems. The first subsystem is a single-component gas which will be either in the BEC or TG regime, while the second subsystem is coupled and can be either in the Composite Fermionization (CF) [27–29], Phase Separation (PS) [26, 30] or Full Fermionization (FF) [52] phase. Thus, these bi-correlated phases will be direct combinations of a BEC or a TG gas with a CF, PS or FF state, as again listed in the left sub-table in Table I. When at least two interspecies coupling strengths tend to infinity, all three components are coupled resulting in the emergence of genuine tri-correlated states that are unique to three-species mixtures and this requires to solve the full many-body Hamiltonian numerically.

TABLE I. The 64 ground-state phases of a three-species mixture of repulsively interacting ultra-cold bosons confined in a one-dimensional harmonic trap. The abbreviations are BEC: Bose–Einstein condensate; TG: Tonks–Girardeau gas; CF: composite fermionization; PS: phase separation; FF: full fermionization; CIB: correlation-induced bunching; CIAB: correlation-induced anti-bunching. The left sub-table shows the phases that can be understood from the solutions of single- and dual-species systems while the right hand side exhibits phases that are unique to the three-species mixture.

	Mono- and Bi-correlated States							Tri-correlated States									
	Name	g_A	g_B	g_C	g_{AB}	g_{AC}	g_{BC}	corner	Name	g_A	g_B	g_C	g_{AB}	g_{AC}	g_{BC}	corner	
	BEC-BEC-BEC	0	0	0	0	0	0	1.1	Triple CF	0	0	0	∞	∞	∞	1.7	
	BEC-BEC-TG	∞	0	0				2.1	CF-PS	∞	0	0				2.7	
		0	∞	0	0	0	0	3.1		0	∞	0	∞	∞	∞	∞	3.7
		0	0	∞				4.1		0	0	∞					4.7
	BEC-TG-TG	∞	∞	0				5.1	Fermionized PS	∞	∞	0				5.7	
		∞	0	∞	0	0	0	6.1		∞	0	∞	∞	∞	∞	∞	6.7
		0	∞	∞				7.1		0	∞	∞					7.7
	TG-TG-TG	∞	∞	∞	0	0	0	8.1	FF	∞	∞	∞	∞	∞	∞	8.7	
	BEC-CF	0	0	0				1.2	CIB type I	0	0	0	∞	0	∞	1.3	
		0	0	0	0	0	∞	1.4		∞	∞	0	∞	∞	0	∞	1.6
		0	0	0	0	∞	0	1.5		0	∞	∞	∞	∞	∞	∞	1.8
	TG-CF	∞	0	0	0	0	∞	2.4	PS	∞	0	0	∞	∞	0	∞	2.6
		0	∞	0	0	∞	0	3.5		0	∞	0	∞	0	∞	∞	3.3
		0	0	∞	∞	0	0	4.2		0	0	∞	0	∞	∞	∞	4.8
	BEC-PS	∞	0	0	∞	0	0	2.2	CIB type II	∞	0	0	∞	0	∞	∞	2.3
		0	∞	0	0	∞	0	2.5		0	∞	0	∞	∞	∞	∞	2.8
		0	∞	0	0	0	∞	3.2		0	∞	0	∞	∞	0	∞	3.6
		0	0	∞	0	∞	0	4.5		0	0	∞	0	∞	∞	0	4.3
		0	0	0	0	0	∞	4.4		∞	∞	0	∞	∞	0	∞	4.6
	TG-PS	∞	∞	0	0	0	∞	5.4	CIAB type I	∞	∞	0	∞	0	∞	∞	5.3
		0	0	∞	0	0	∞	5.5		∞	∞	0	∞	∞	0	∞	5.6
		∞	0	∞	0	0	∞	6.4		∞	0	∞	∞	∞	0	∞	6.6
		0	∞	∞	0	0	0	6.2		0	0	∞	∞	∞	∞	0	6.8
		0	∞	∞	0	∞	0	7.2		0	∞	∞	0	∞	0	∞	7.3
	BEC-FF	∞	∞	0	∞	0	0	5.2	CIB type III	∞	∞	0	0	∞	∞	∞	5.8
		∞	0	∞	0	∞	0	6.5		∞	0	∞	∞	0	∞	∞	6.3
		0	∞	∞	0	0	∞	7.4		0	∞	∞	∞	∞	0	∞	7.6
	TG-FF	∞	∞	∞	∞	0	0	8.2	CIAB type II	∞	∞	∞	∞	0	∞	∞	8.3
		0	0	0	0	0	∞	8.4		0	∞	∞	∞	∞	0	∞	8.6
		0	0	0	0	0	∞	8.5		0	∞	∞	∞	∞	∞	∞	8.8

B. Methodology

While accurately solving the many-body Schrödinger equation is paramount when exploring correlations in complex interacting quantum systems, it is a computational challenge due to the usually large Hilbert space. In this work we employ the improved Exact Diagonalization method [32] to numerically diagonalize the Hamiltonian (1) and obtain the ground state of the system in the different parameter regimes. Since we are treating quantum systems consisting of identical particles, it is convenient to rewrite the Hamiltonian (1) in the second-quantized formalism by introducing the σ -component bosonic annihilation operator $\hat{a}_{\sigma,k}$ as

$$\hat{a}_{\sigma,k} = \int \phi_{\sigma,k}^*(x) \hat{\Psi}_{\sigma}(x) dx, \quad (4)$$

where $\hat{\Psi}_{\sigma}(x) = \sum_k \phi_{\sigma,k}(x) \hat{a}_{\sigma,k}$ denotes the bosonic field operator that annihilates a σ -species boson in the single-particle state $\phi_{\sigma,k}(x)$ at position x . As usual, the annihilation operator $\hat{a}_{\sigma,k}$ and its corresponding creation operator $\hat{a}_{\sigma,\ell}^{\dagger}$ must satisfy the commutation relations

$$[\hat{a}_{\sigma,k}, \hat{a}_{\sigma',\ell}^{\dagger}] = \delta_{\sigma\sigma'} \delta_{k\ell}, \quad (5)$$

$$[\hat{a}_{\sigma,k}^{\dagger}, \hat{a}_{\sigma',\ell}^{\dagger}] = [\hat{a}_{\sigma,k}, \hat{a}_{\sigma',\ell}] = 0. \quad (6)$$

The many-body Hamiltonian can then be transformed into

$$\hat{H} = \sum_{\sigma \in \{A, B, C\}} \left[\sum_{k, \ell} h_{k\ell}^{\sigma} \hat{a}_{\sigma, k}^{\dagger} \hat{a}_{\sigma, \ell} + \frac{1}{2} \sum_{k\ell mn} W_{k\ell mn}^{\sigma} \hat{a}_{\sigma, k}^{\dagger} \hat{a}_{\sigma, \ell}^{\dagger} \hat{a}_{\sigma, m} \hat{a}_{\sigma, n} \right] + \sum_{\sigma \neq \delta \in \{A, B, C\}} \sum_{k\ell mn} W_{k\ell mn}^{\sigma\delta} \hat{a}_{\sigma, k}^{\dagger} \hat{a}_{\delta, \ell}^{\dagger} \hat{a}_{\sigma, m} \hat{a}_{\delta, n}, \quad (7)$$

where $h_{k\ell}^{\sigma}$ denotes the σ -component one-body matrix elements, while $W_{k\ell mn}^{\sigma}$, and $W_{k\ell mn}^{\sigma\delta}$ are the intra- and interspecies two-body matrix elements, respectively. Explicitly they are given as

$$h_{k\ell}^{\sigma} = \int \phi_{\sigma, k}^{*}(x^{\sigma}) \left[-\frac{1}{2} \frac{d^2}{d(x^{\sigma})^2} + \frac{1}{2} (x^{\sigma})^2 \right] \phi_{\sigma, \ell}(x^{\sigma}) dx^{\sigma}, \quad (8)$$

$$W_{k\ell mn}^{\sigma} = g_{\sigma} \iint \phi_{\sigma, k}^{*}(x_1^{\sigma}) \phi_{\sigma, \ell}^{*}(x_2^{\sigma}) \delta(x_1^{\sigma} - x_2^{\sigma}) \phi_{\sigma, m}(x_1^{\sigma}) \phi_{\sigma, n}(x_2^{\sigma}) dx_1^{\sigma} dx_2^{\sigma}, \quad (9)$$

$$W_{k\ell mn}^{\sigma\delta} = g_{\sigma\delta} \iint \phi_{\sigma, k}^{*}(x^{\sigma}) \phi_{\delta, \ell}^{*}(x^{\delta}) \delta(x^{\sigma} - x^{\delta}) \phi_{\sigma, m}(x^{\sigma}) \phi_{\delta, n}(x^{\delta}) dx^{\sigma} dx^{\delta}. \quad (10)$$

In this work, we use the harmonic oscillator eigenfunctions as the single-particle functions $\phi_{\sigma, k}(x)$ since this choice not only makes $h_{k\ell}^{\sigma} = \left(k + \frac{1}{2}\right) \delta_{k\ell}$ diagonal, but also allows us to employ the effective-interaction approach that incorporates the exact two-particle solutions [53] for obtaining $W_{k\ell mn}^{\sigma}$ and $W_{k\ell mn}^{\sigma\delta}$ instead of directly evaluating integrals given by Eqs. (9) and (10). This regularized strategy has been widely used in previous works and it has been thoroughly shown that it gives a better convergence in the case of the Fermi-Huang pseudo-potential δ -function [32, 54–57]. A comprehensive comparison of various regularized strategies in one-dimensional few-body systems can be found in a recent work [58].

We solve the many-body Hamiltonian by expanding the trial wavefunction (ansatz) into a linear combination of a set of orthonormal Fock states associated with the expansion coefficients c_{j_A, j_B, j_C} as

$$|\Psi\rangle = \sum_{j_A=1}^{D_A} \sum_{j_B=1}^{D_B} \sum_{j_C=1}^{D_C} c_{j_A, j_B, j_C} |n^A\rangle_{j_A} |n^B\rangle_{j_B} |n^C\rangle_{j_C} = \sum_{J=1}^D c_J |J\rangle. \quad (11)$$

where $|n^{\sigma}\rangle_{j_{\sigma}} = |n_1^{\sigma}, n_2^{\sigma} \dots n_i^{\sigma} \dots\rangle$ denotes a possible σ -component permanent with n_i^{σ} being the occupation number of σ -type bosons occupying the single-particle state $\phi_{\sigma, k}(x)$. The occupation numbers can be positive integers varying between 0 and N_{σ} and satisfy the condition $\sum_i n_i^{\sigma} = N_{\sigma}$. For brevity, we use a composite index such that $c_J = c_{j_A, j_B, j_C}$

and $|J\rangle = |n^A\rangle_{j_A} |n^B\rangle_{j_B} |n^C\rangle_{j_C}$. For numerical reasons the many-body Fock basis has to be truncated such that a sufficiently large but finite Hilbert space is used and the total number of Fock states in the expansion is $D = D_A \cdot D_B \cdot D_C$ with D_{σ} being the number of σ -species Fock states. In this work we use an efficient truncation scheme proposed in Refs. [59, 60] to determine the value of D , which limits the many-body Fock states $|J\rangle$ in the expansion to ones that have an energy smaller than a certain optimal value E_{opt} . This allows one to control the accuracy of the numerical results by varying E_{opt} . This technique can be applied to both bosonic and fermionic systems and has been widely used in recent years [32, 38, 57, 61–65]. To make the calculations in the present work feasible, we use another technique that significantly reduces the dimension of the truncated Hilbert by selecting dominant configurations with respect to the spatial symmetry of the desired many-body state [32]. If the trapping potential is spatially symmetric

$$V(x) = V(-x), \quad (12)$$

the single-particle eigenfunctions $\phi_n(x)$ have a well-defined parity given by

$$\hat{P}\phi_n(x) = p\phi_n(-x), \quad (13)$$

where \hat{P} is the symmetry operator whose eigenvalues are $p = \pm 1$. The single-particle functions $\phi_n(x)$ with $p = 1$ are spatially symmetric or even functions, while those with $p = -1$ are spatially antisymmetric or odd functions. Since the Fock states are constructed as the symmetrized Hartree product of the single-particle functions, they also satisfy this spatial symmetry. This allows us to classify the Fock states into two categories according to their spatial symmetries: even- and odd-parity Fock states. As a consequence, the many-body wave functions only span in one of these subspaces. Therefore, in practice, an ansatz can be constructed only from Fock states that have the same parity as the desired many-body wavefunction. In the present work we focus on the ground state of multi-species few-boson systems that is spatially symmetric, therefore only Fock states $|J\rangle$ with even-parity symmetry contribute

to the many-body wave function while the odd-parity Fock states can be safely excluded from the calculations. Since we focus on studying the stationary properties, the problem of variationally finding the expansion coefficients c_J such that the expectation value of the Hamiltonian (7) is minimized with respect to the ansatz (11) now leads to a standard Hermitian eigenvalue problem which can be written as

$$\mathcal{H}|C_m\rangle = E_m|C_m\rangle, \quad (14)$$

where $\mathcal{H} = \langle I|\hat{H}|J\rangle$ is the matrix representation of the many-body Hamiltonian (7). The m -th eigenvalue is given by E_m and the corresponding eigenvector $|C_m\rangle$ is a column vector storing the expansion coefficients c_J . So far this improved scheme has been employed in our previous works [32, 38].

C. Quantities of interest

Having obtained the full many-body wavefunction for a given set of parameters, we are able to investigate all static properties of the ground-state. One of the first quantities of interest is the reduced one-body density matrix (OBDM), which describes the probability to find a σ -component boson at x' after being measured at x . It is given by

$$\rho_\sigma^{(1)}(x, x') = \langle \Psi | \hat{\Psi}_\sigma^\dagger(x) \hat{\Psi}_\sigma(x') | \Psi \rangle, \quad (15)$$

where $|\Psi\rangle$ is the ground-state wavefunction of the system. The ascendingly sorted eigenvalues λ_j^σ of the OBDM describe the occupations of the corresponding natural orbitals and characterize the coherence/fragmentation according to Penrose-Onsager criterion [66]. Furthermore, the diagonal of the OBDM defines the one-body density distribution

$$\rho_\sigma^{(1)}(x) = \langle \Psi | \hat{\Psi}_\sigma^\dagger(x) \hat{\Psi}_\sigma(x) | \Psi \rangle, \quad (16)$$

which can be used to assess the spatial distribution of the three individual components. Spatial correlations can be further characterized by the intra- and interspecies two-body correlation functions (TBCF) which are respectively defined as

$$\rho_\sigma^{(2)}(x_1, x_2) = \langle \Psi | \hat{\Psi}_\sigma^\dagger(x_1) \hat{\Psi}_\sigma^\dagger(x_2) \hat{\Psi}_\sigma(x_1) \hat{\Psi}_\sigma(x_2) | \Psi \rangle, \quad (17)$$

$$\rho_{\sigma\delta}^{(2)}(x^\sigma, x^\delta) = \langle \Psi | \hat{\Psi}_\sigma^\dagger(x^\sigma) \hat{\Psi}_\delta^\dagger(x^\delta) \hat{\Psi}_\sigma(x^\sigma) \hat{\Psi}_\delta(x^\delta) | \Psi \rangle. \quad (18)$$

The physical meaning of $\rho_\sigma^{(2)}(x_1, x_2)$ is the joint probability of finding one σ -species boson at position x_1 and the other of the same species at x_2 . Similarly, $\rho_{\sigma\delta}^{(2)}(x^\sigma, x^\delta)$ has the same meaning as $\rho_\sigma^{(2)}(x_1, x_2)$, but for two bosons of different species. It is worth noting that these spatial correlations functions can be experimentally measured via the time-of-flight absorption imaging technique [18, 67, 68]. To maintain consistency we will in the following normalize all density profiles to each component's respective particle number and all spatial density matrices to unity.

To quantify the inter- and intraspecies correlations present in our system, including correlations that arise from direct interactions between particles from the same species and correlations that are induced by the couplings to other species, we evaluate the inter- and intraspecies bipartite mutual informations (BMI) respectively defined as

$$I_{\sigma\delta} = S_{\sigma\sigma} + S_{\delta\delta} - S_{\gamma\gamma}, \quad (19)$$

$$I_\sigma = 2S_\sigma - S_{\sigma\sigma}. \quad (20)$$

It is noted that $S_\sigma = -\text{tr}[\tilde{\rho}_\sigma \log_2(\tilde{\rho}_\sigma)]$ and $S_{\sigma\delta} = -\text{tr}[\tilde{\rho}_{\sigma\delta} \log_2(\tilde{\rho}_{\sigma\delta})]$ respectively are the single- and two-particle von Neumann entropy. Here $\tilde{\rho}_\sigma$ denotes the reduced one-body density matrix of one σ -species boson and $\tilde{\rho}_{\sigma\delta}$ denote the reduced two-body density matrix of one σ -species and one δ -species bosons after tracing out the remaining system. It is worth mentioning that the BMI is always non-negative [69].

III. RESULTS AND DISCUSSION

A. Tri-correlated states

All tri-correlated states that emerge in the interacting three-species mixture are listed and defined on the right hand side of Table I. In the following we focus on three representative cases of this group: the Fermionized Phase Separation case (Fermionized PS), the Correlation-induced Anti-bunching Type I case (CIAB Type I), and the Correlation-induced Bunching Type II case (CIB Type II). The label of the corner from Fig. 1 for each particular case to be discussed below is indicated by the red color in Table I. We will show that these phases possess interesting long-range correlations or spatial self-localization due to the presence of the third species. The remaining tri-correlated states (indicated by the green color in Table I) are presented in Appendix A.

1. Fermionized Phase Separation

The first case we discuss is termed ‘‘Fermionized Phase Separation’’ and it appears at the corners 5.7, 6.7 and 7.7 in Fig. 1. As the representative we discuss corner 5.7, which corresponds to the interaction strengths $g_A = g_B = g_{AB} = g_{BC} = g_{AC} \rightarrow \infty$, and $g_C = 0$. The corresponding ground-state density profiles are shown in Figs. 2(a-c), and one can immediately see that the C species occupies the center of the trap, while the A and B species are spatially separated to the left and right edges of the trap. This is very similar to the phase separation case in binary bosonic mixtures [30], and can be straightforwardly understood by realising that the interaction energy is minimized when the species with zero intraspecies interactions is localized in the high-density trap center, while the species with repulsive intraspecies interactions achieve lower densities by splitting and reducing the overlap of the two particles.

However, this case distinguishes itself from the phase separation case in binary mixtures as the overlapping parts of A and B are fermionized. To fully understand the behavior of the two A and two B atoms in this case, it is necessary to examine their OBDMs (Figs. 2(d-f)) and TBCFs (Figs. 2(g-l)). While the OBDMs clearly show the splitting of the A and B components, the TBCFs show how the particles in each component are organized. For instance, for the A component there are both anti-correlated contributions, where the particles of A are split on either side of C, and correlated contributions, where both particles of A are bunched together on one side of C. For the latter the effects of the strong intraspecies interactions are clearly seen in the vanishing of the diagonal contribution. The TBCF for the B particles is exactly the same, and so is the interspecies TBCF $\rho_{AB}^{(2)}$, showing that the A and B particles sit on top of each other in a fully fermionized state. We note that since all interaction strengths are the same, the A-B system is SU(2) symmetric and thus any A particle can be swapped with a B particle. Therefore, any distribution of two particles on each side of C would have the same energy.

To understand the coherence and correlation properties of the ground state we look at the eigenvalues of the OBDMs shown in Fig. 2(m). The A(B) species can be seen to be fragmented with the eigenvalues being nearly doubly degenerate due to the spatial splitting into a superposition state between the left and right hand side of the harmonic trap. This indicates that the A and B species both possess strong intra- and interspecies correlations that can be quantified by their high mutual information $I_{A(B)}$ and I_{AB} shown in Figs. 2(n,o). Meanwhile, the C component remains mostly coherent with one dominant eigenvalue $\lambda_1^C \approx 0.9$. However, a second relevant eigenvalue $\lambda_2^C \approx 0.1$ is also visible, despite the absence of an intraspecies interaction between C-type bosons. This is consistent with the mutual information I_C also having a finite value, indicating that the two C atoms are actually correlated (see Fig. 2(n)), which stems from the induced effective attractive interactions through the interspecies couplings to the A and B species which weakly binds the C particles as shown in Figs. 2(f,i). Finally, one can see that the C species is less correlated with the A(B) species as there is reduced overlap between the states due to phase separation and therefore the interspecies mutual information takes comparatively small values.

2. Correlation-induced Anti-bunching Type I

The second phase of interest is the ‘‘Correlation-induced Anti-bunching Type I’’ phase, of which there are six realisations (see Table. I). In Fig. 3 we show the results for the ground state for the representative case with the interaction configuration $g_A = g_B = g_{AB} = g_{AC} \rightarrow \infty$, and $g_C = g_{BC} = 0$, which corresponds to the corner 5.6 in Fig. 1. While for this set of interaction strengths the TG pairs of A and B atoms would demonstrate full fermionization in the absence of the third species, the different interactions with the C species leads to a completely different behaviour. From Figs. 3(a-c) one can immediately see that the species B and C locate in the the center of the trap, while species A is anti-bunched due to its strong repulsive intraspecies interactions and located at the edges with one atom on each side of the central clouds (see Fig. 3(g)). The spatial superposition state formed by species A can also be seen in the doubly-degenerate natural occupation numbers, in which the two largest values are close to 0.5 [70], while the large value of I_A in Fig. 3(n) shows the strong intraspecies correlations as expected. Meanwhile species C remains mostly coherent with the largest natural occupancy being close to one, which is consistent with its Gaussian-like correlation functions depicted in Figs. 3(f,i), which only evinces weak induced intraspecies correlations via the coupling to species A as can be seen from I_C slightly deviating from zero in Fig. 3(n).

The most remarkable self-organization effect of this case is that species B is located in the center of the trap despite its strongly repulsive intraspecies interaction. While it forms a localized TG state, one can see in Fig. 3(b) that the width of $\rho_B^{(1)}(x)$ is noticeably smaller than that of the conventional TG pair in a harmonic trap [51], seemingly due to the repulsive pressure from the A species atoms. This is also confirmed by the one- and two-body correlation functions shown in Figs. 3(e,h). However, we point out that the correlations between the B particles are noticeably reduced when compared to two TG particles in a harmonic oscillator (see Fig. 3(n)) in which case $I_B \approx 1.97$ [70], as the large coupling to the A component is responsible for screening the correlations between the B particles. Indeed, the A

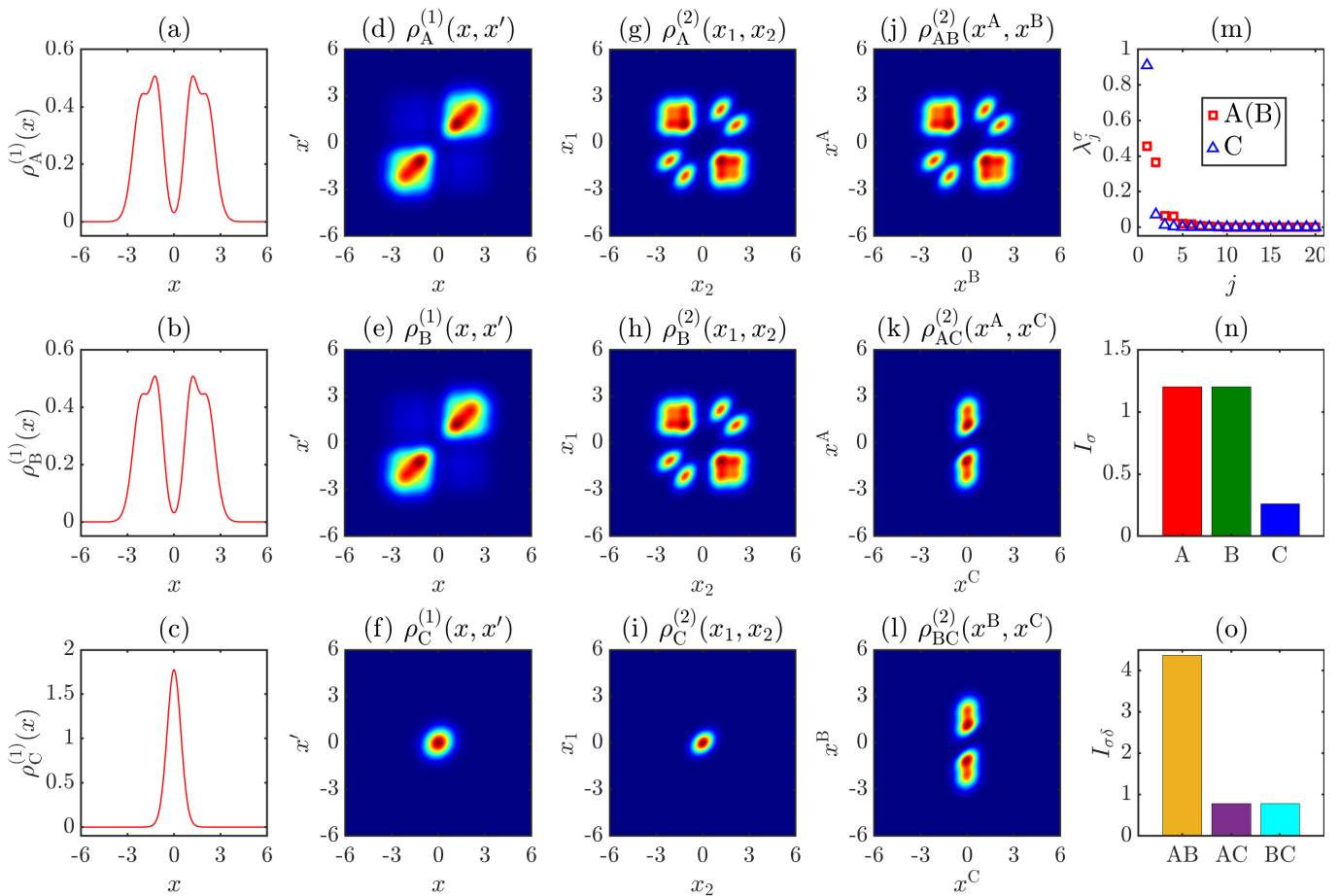


FIG. 2. The ‘Fermionized Phase Separation’ phase ($g_A = g_B = g_{AB} = g_{BC} = g_{AC} \rightarrow \infty$, $g_C = 0$). (a-c) The one-body density distribution function $\rho_\sigma^{(1)}(x)$. (d-f) The one-body density matrix $\rho_\sigma^{(1)}(x, x')$. (g-i) The intraspecies two-body correlation function $\rho_\sigma^{(2)}(x_1, x_2)$. (j-l) The interspecies two-body correlation function $\rho_{\sigma\delta}^{(2)}(x^\sigma, x^\delta)$. (m) The eigenvalues λ_j^σ of the one-body density matrices. (n) The intraspecies mutual information I_σ . (o) The interspecies mutual information $I_{\sigma\delta}$.

and B components are strongly correlated, as seen in Fig. 3(o), which, due to entanglement monogamy, reduces the correlations in B [71]. Finally, the correlations between B and C are non-zero even though they are not directly coupled ($g_{BC} = 0$), which is again due to induced correlations from their mutual coupling to the A species. Intriguingly, a phase referred to as Correlation-induced Anti-bunching Type II, exhibiting a quite similar properties to this phase, is addressed in the appendix A 5.

3. Correlation-induced Bunching Type II

While the two phases discussed above both show splitting between infinitely repulsively interacting bosons, we discuss next a phase that is dominated by completely different physics stemming from the presence of induced attractive interactions, that can lead to stronger localisation of non-interacting bosons. This case of interest is named ‘Correlation-induced Bunching Type II’, and corresponds to systems where only one intraspecies coupling strength is infinite, and this component decouples from one of the other components. All other interspecies coupling strengths are infinite, which means that there are six realisations of this case (see Table. I). Here, we will discuss the example where the B component has strong intraspecies interactions, but does not interact with the C component, i.e. $g_{AB} = g_{AC} = g_B \rightarrow \infty$, and $g_A = g_C = g_{BC} = 0$ (the corner 3.6).

From Fig. 4, it can be seen that the strong intraspecies interactions for species B the B atoms does not want to be located in the center of the trap, however it also does not want to overlap with the A component. One can see in Figs. 4(a-c) that this leads to a situation where species B exhibits a unique density profile due to these competing interactions, possessing a Gaussian like peak around $x = 0$ which noticeably widens around the half maximum into

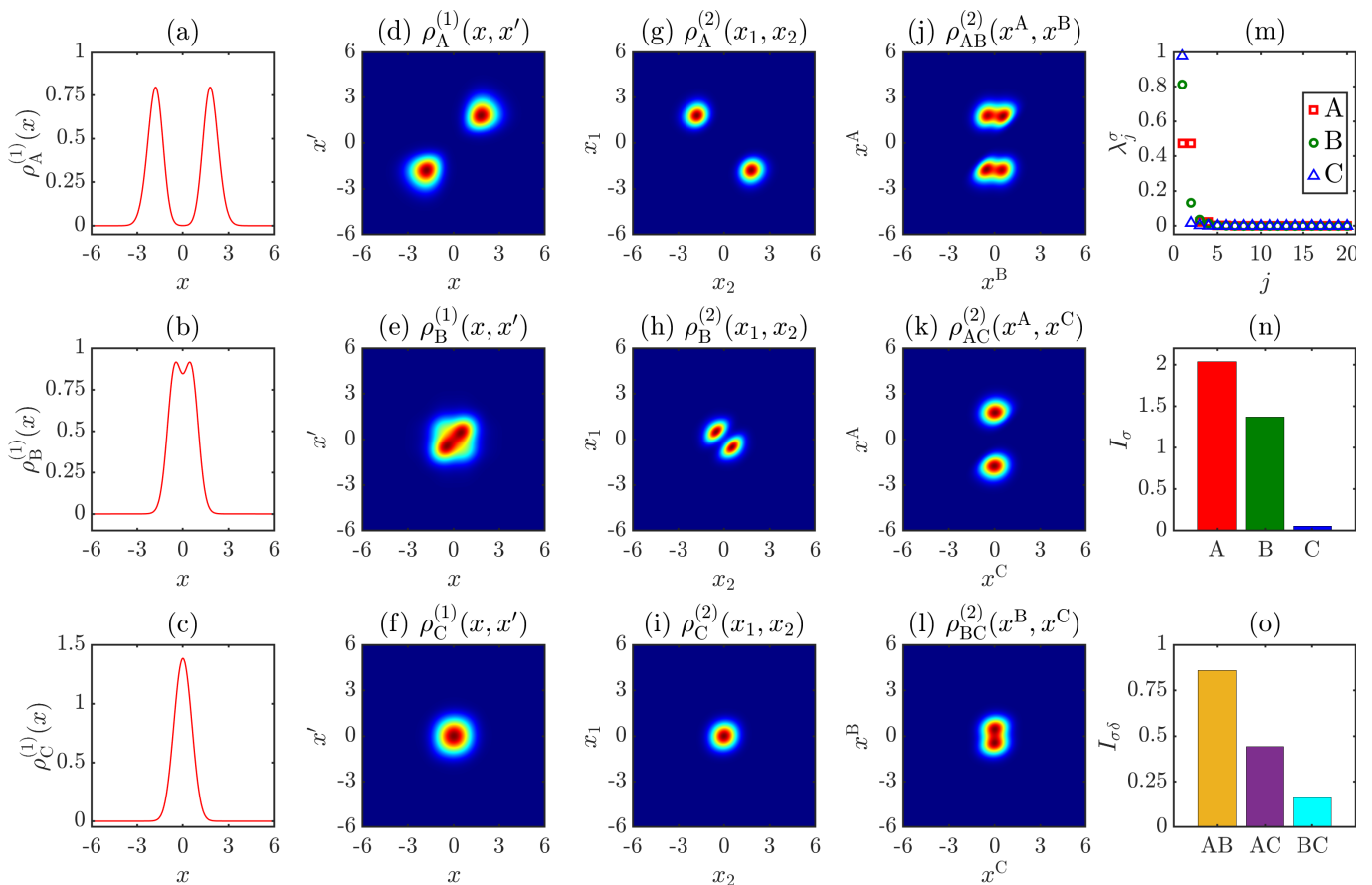


FIG. 3. The ‘Correlation-induced Anti-bunching Type I’ phase ($g_A = g_B = g_{AB} = g_{AC} \rightarrow \infty$, and $g_C = g_{BC} = 0$). (a-c) The one-body density distribution function $\rho_{\sigma}^{(1)}(x)$. (d-f) The one-body density matrix $\rho_{\sigma}^{(1)}(x, x')$. (g-i) The intraspecies two-body correlation function $\rho_{\sigma}^{(2)}(x_1, x_2)$. (j-l) The interspecies two-body correlation function $\rho_{\sigma\delta}^{(2)}(x^{\sigma}, x^{\delta})$. (m) The eigenvalues λ_j^{σ} of the one-body density matrices. (n) The intraspecies mutual information I_{σ} . (o) The interspecies mutual information $I_{\sigma\delta}$.

distinct shoulders. This shape is the consequence of the competition between the pressure from the A component to phase separate and the intraspecies interaction to expand to allow the B atoms to decrease their overlap with each other. The TBCF of species B, $\rho_B^{(2)}(x_1, x_2)$ shows a zero along the diagonal due to the fact that the two B atoms cannot be in the same place simultaneously, but also highlights a non-trivial ordering of the B particles. If one B particle is localized at the trap minimum $x = 0$, the other B particle will be localized in a superposition of being to the left and right of it. This therefore leads to the fact that the B bosons are more strongly correlated than A bosons, which only possess bunching correlations. Indeed, components A and C behave very similarly to those in the ‘Correlation-induced bunching type I’ case described in the appendix A 6. In Fig. 4(o) we can see $I_{AB} > I_{AC} > I_{BC}$, which shows that the components A and B have the highest interspecies correlations due to the increased overlap, while the components B and C have the lowest interspecies correlations as they are induced only. Note that if the C species also has intraspecies interactions, i.e. $g_{AB} = g_{AC} = g_C = g_B \rightarrow \infty$, and $g_A = g_{BC} = 0$ (the corner 7.6), the system exhibits the Correlation-induced Bunching Type III which is presented in the appendix A 7.

B. Crossover between phases

While the corners of the hypercube most clearly indicate the different possible phases, there is a large state space in between where the interaction strengths can be finite. The crossover region between two corners will therefore be non-trivial, particularly if the limits are strongly correlated states. We will focus on two specific examples, the first when the corner states are associated with strongly correlated fully-fermionized states, and the second when the corner states are associated with bunching correlations.

As a representative example we therefore look at the Fermionized Phase Separation phase and consider the direct

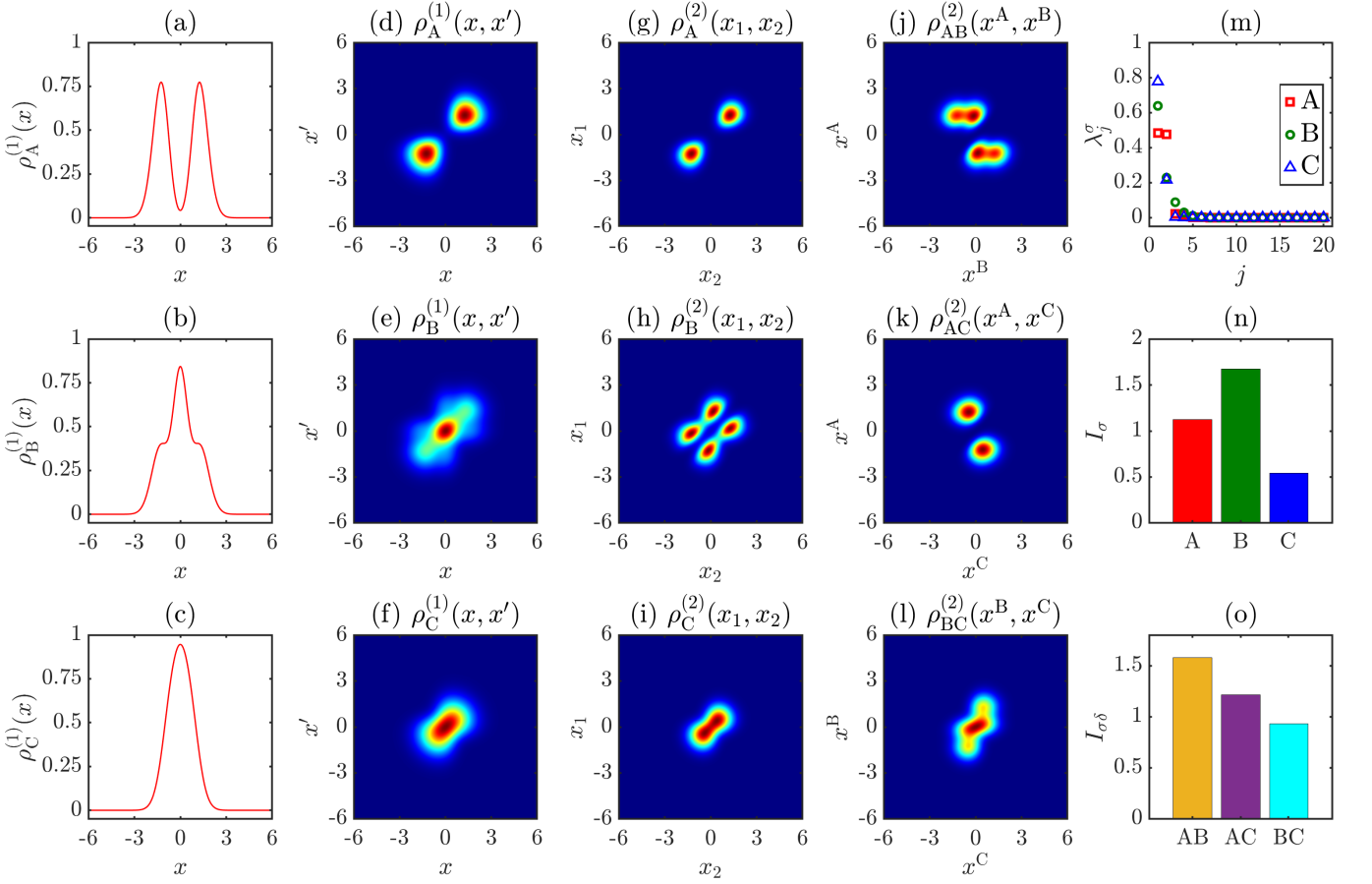


FIG. 4. The ‘Correlation-induced Bunching Type II’ phase ($g_{AB} = g_{AC} = g_B \rightarrow \infty$, and $g_A = g_C = g_{BC} = 0$). (a-c) The one-body density distribution function $\rho_\sigma^{(1)}(x)$. (d-f) The one-body density matrix $\rho_\sigma^{(1)}(x, x')$. (g-i) The intraspecies two-body correlation function $\rho_\sigma^{(2)}(x_1, x_2)$. (j-l) The interspecies two-body correlation function $\rho_{\sigma\delta}^{(2)}(x^\sigma, x^\delta)$. (m) The eigenvalues λ_j^σ of the one-body density matrices. (n) The intraspecies mutual information I_σ . (o) The interspecies mutual information $I_{\sigma\delta}$.

connection between the corners 5.7 and 6.7. This corresponds to increasing $g_C = 0 \rightarrow \infty$ while simultaneously decreasing $g_B = \infty \rightarrow 0$. Along this trajectory strong interspecies correlations will be swapped from the A-B pair to the A-C pair. Since numerically we only treat the strong interactions up to $g = 20$, we show in Fig. 5 the corresponding results as a function of increasing $g_C = g = 0 \rightarrow 20$, while $g_B = 20 - g_C$. The spatial one-body density distribution functions $\rho_\sigma^{(1)}(x)$ are shown in the first row of Fig. 5. As already discussed in Fig. 2 both species A and B are in a phase-separated fully fermionized state and are located at the edges of the trap for $g = 0$, while species C is tightly localized in the center. Once the coupling strength g increases, species A and B continue being split until $g \approx 8$, and indeed their densities completely overlap up until this point. This can be quantified by the overlap between the one-body distribution of two species, $\rho_\sigma^{(1)}(x)$ and $\rho_\delta^{(1)}(x)$, which is given by

$$\mathcal{O}_{\sigma\delta} = \left| \int \sqrt{\rho_\sigma^{(1)}(x)\rho_\delta^{(1)}(x)} dx \right|^2. \quad (21)$$

This will be unity if two species are exactly superimposed, as shown for the A and B species in Fig. 5(f) for $g \lesssim 8$. For larger interactions there is a crossover region where the B particles swap positions with the C particles, and for interactions $g \gtrsim 12$ the A and C species have maximum overlap.

While the density and its overlap can give some idea of the re-organization of the particles, it contains no information about the position of particles with respect to one another, i.e. whether they are bunched or anti-bunched as described by the TBCF. The crossover between anti-bunching and bunching correlations in species σ can be well

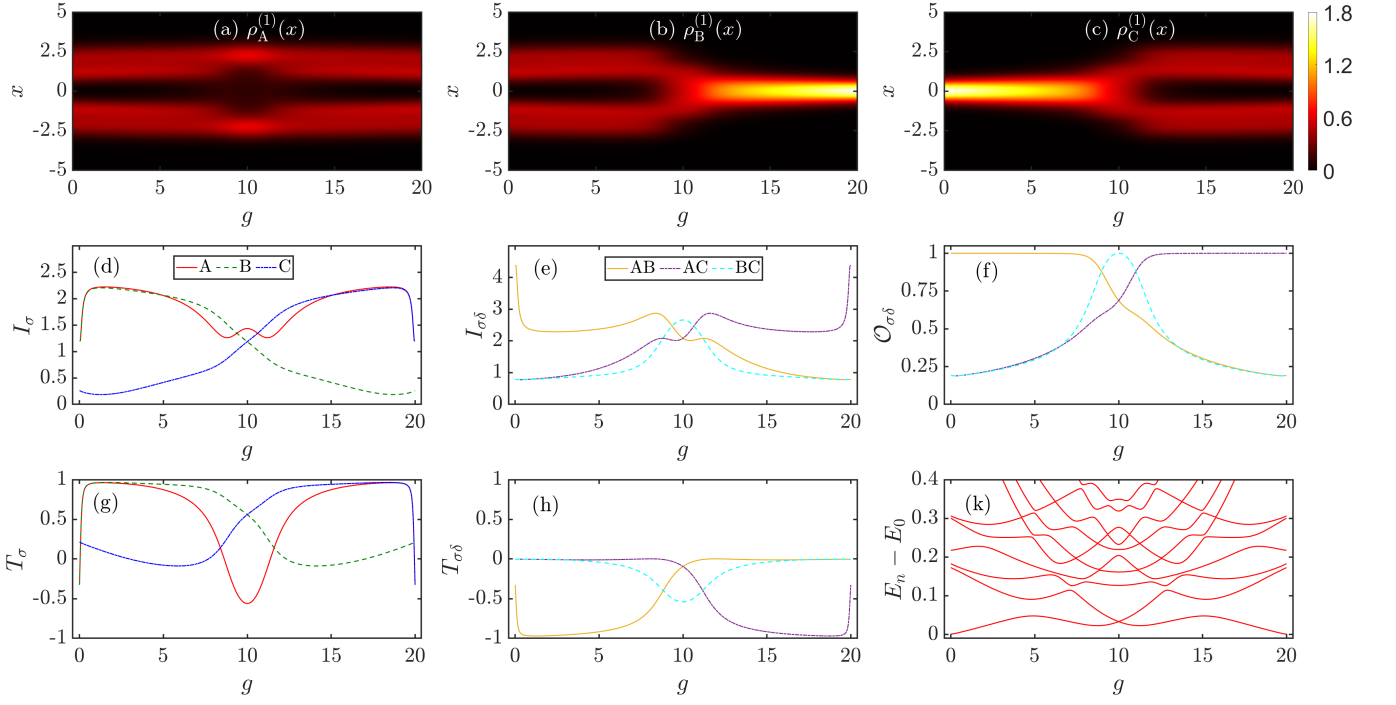


FIG. 5. (a-c) The spatial one-body density distribution function $\rho_\sigma^{(1)}(x)$. (d) The intraspecies mutual information I_σ . (e) The interspecies mutual information $I_{\sigma\delta}$. (f) The density overlap $\mathcal{O}_{\sigma\delta}$. (g) The intraspecies correlation crossover T_σ . (h) The interspecies correlation crossover $T_{\sigma\delta}$. (k) The even-parity excitation energy spectrum $E_n - E_0$. Note that $g_C = g$ while $g_B = 20 - g$.

quantified by the intraspecies two-particle coincidence function

$$T_\sigma = \iint_{x_1 \cdot x_2 > 0} \rho_\sigma^{(2)}(x_1, x_2) dx_1 dx_2 - \iint_{x_1 \cdot x_2 < 0} \rho_\sigma^{(2)}(x_1, x_2) dx_1 dx_2 \quad (22)$$

which compares the probability of finding two σ -type particles being bunched (the first integral) with being anti-bunched (the second integral). It should be remarked that the quadrant defined by the condition $x_1 \cdot x_2 > 0$ encompasses two spatial regions where the variables x_1 and x_2 have the same sign, specifically $(x_1 < 0, x_2 < 0)$ and $(x_1 > 0, x_2 > 0)$, illustrating bunching correlations. Meanwhile, the quadrant satisfies the condition $x_1 \cdot x_2 < 0$ corresponding the area where the variables x_1 and x_2 have the opposite sign, showing anti-bunching correlations. If $T_\sigma > 0$ ($T_\sigma < 0$) the bunching (anti-bunching) correlations are more dominant than the anti-bunching (bunching) ones, while two σ -species particles are said to be fully bunched if $T_\sigma = 1$, and fully anti-bunched if $T_\sigma = -1$. In Fig. 5(g) we show the intraspecies two-particle coincidence function as a function of g . The initial state at $g = 0$ is slightly more anti-bunched in the A and B components (see Fig. 2), however they become maximally bunched for small and finite $g > 0$. In this case when the symmetry between the A and B species is slightly broken ($g_A \neq g_B$) particles of the same species will more likely stay together, but still bisected by the C component. Interestingly, the opposite effect is seen in the interspecies two-particle coincidence function, which can similarly characterized by

$$T_{\sigma\delta} = \iint_{x^\sigma \cdot x^\delta > 0} \rho_{\sigma\delta}^{(2)}(x^\sigma, x^\delta) dx^\sigma dx^\delta - \iint_{x^\sigma \cdot x^\delta < 0} \rho_{\sigma\delta}^{(2)}(x^\sigma, x^\delta) dx^\sigma dx^\delta. \quad (23)$$

This function is shown in Fig. 5(h) and it is similarly slightly anti-bunched at $g = 0$ for an A-B pair, since the inter- and intraspecies TBCFs are identical in this case (see Fig. 2(g,j,h)). When the symmetry is broken the A and B species maximally anti-bunch with respect to one another, i.e. if an A particle is found on the left-side of the trap, a B particle will be found on the right-side of the trap. The tendency of the particles to bunch or anti-bunch is also echoed in the intra- and interspecies mutual information as shown in Fig. 5(d) and Fig. 5(e) respectively. For example, the bunching of A particles leads to an increase in their intraspecies mutual information, while the anti-bunching between A and B particles reduces their interspecies mutual information. We also note that around the crossover region, at $g \approx 10$, where all species have a large overlap with one another, all pairs of particles have approximately the

same mutual information, indicating pair correlations are spread equally among all components. This saturation of two-body correlations means that three-body correlations between all the components effectively vanish throughout the crossover.

Finally, we remark on the the energy spectrum of the low-lying excited states for the presented model in Fig. 5(k). As can be seen clearly, the energy spectrum exhibits a number of avoided crossings, in particular between the ground-state and the even-parity first excited state. Furthermore, the spectrum also features several crossings, especially at the point $g = 10$. Such the complex spectrum suggest that driving the systems diabatically would result in the creation of irreversible excitations to higher energy states, which could pose a problem for the control of multi-species systems.

IV. CONCLUSION AND OUTLOOK

In this work we have systematically laid the foundations for understanding quantum correlations, coherences and spatial localization of one-dimensional three-species mixtures of ultra-cold few bosons confined harmonically. Our calculations are based on the improved Exact Diagonalization scheme that efficiently solves the many-body Schrödinger equation of mixtures of a few interacting indistinguishable particles in a truncated Hilbert space. This numerical tool has allowed us to calculate the full many-body ground-state wavefunction and thus explore all possible quantum correlations, coherence, spatial self-localization and entanglement. From this insight we have categorised all phases by their inter- and intraspecies coupling strengths, focusing on the limits of either the ideal ($g = 0$) or the hard-core ($g \rightarrow \infty$) behaviour. We have found ten ground-state phases that are unique to three-species mixtures of interacting bosons, three of which are discussed in the main text and the remaining seven in the Appendix for completeness. It is worth mentioning that the “Full Fermionization” phase (see Appendix A 2) has $SU(3)$ symmetry, while the other phases do not have this symmetry. Therefore these phases can be mapped into an effective spin model as it has been done in binary mixtures in the strongly interacting regime with $SU(2)$ symmetry [72–76]. Furthermore, we have also discussed the crossover between two related corner states by changing two intraspecies coupling strengths concurrently. The results show that although the correlations can be exchanged between two species, it strongly depends on the particle-particle interactions. Some correlation exchanges between two species may be more difficult to obtain in practice since the system needs driving through a quantum-matter barrier formed by the third component. This naturally gives rise to a fundamental and interesting question about the design of geodesic paths for driving quantum many-body systems to the desired state that will be addressed in future work [77, 78]. In addition to the above results it would be interesting to study mass- or particle-imbalanced systems, transitions between different correlated phases and also non-equilibrium dynamics along with the investigation of the emergence of quantum chaos. Furthermore, it will be interesting to derive a variational ansatz for each of the new phases that are unique to the three-species strongly-correlated system.

ACKNOWLEDGMENTS

The work is supported by the Okinawa Institute of Science and Technology Graduate University (OIST). All numerical simulations were performed on the high-performance computing cluster provided by the Scientific Computing and Data Analysis section at OIST. T.B., T.F., and T.D.A.-T. acknowledge support from JST COI-NEXT Grant No. JPMJPF2221 and T.F. is also supported by JSPS KAKENHI Grant No. JP23K03290. T.D.A.-T. thanks the Pure and Applied Mathematics University Research Institute at the Polytechnic University of Valencia for their kind hospitality. M.A.G.-M is supported by the Ministry for Digital Transformation and of Civil Service of the Spanish Government through the QUANTUM ENIA project call - Quantum Spain project, and by the European Union through the Recovery, Transformation and Resilience Plan - NextGenerationEU within the framework of the Digital Spain 2026 Agenda: also from Projects of MCIN with funding from European Union NextGenerationEU (PRTR-C17.I1) and by Generalitat Valenciana, with Ref. 20220883 (PerovsQuTe) and COMCUANTICA/007 (QuanTwin), and Red Tematica RED2022-134391-T.

Appendix A: Additional Tri-correlated States

1. Triple Composite Fermionization

The case where all three interspecies coupling strengths tend to infinity while all intraspecies ones are equal to zero is termed “Triple Composite Fermionization” and corresponds to the corner 1.7 in Fig. 1. Since all species strongly

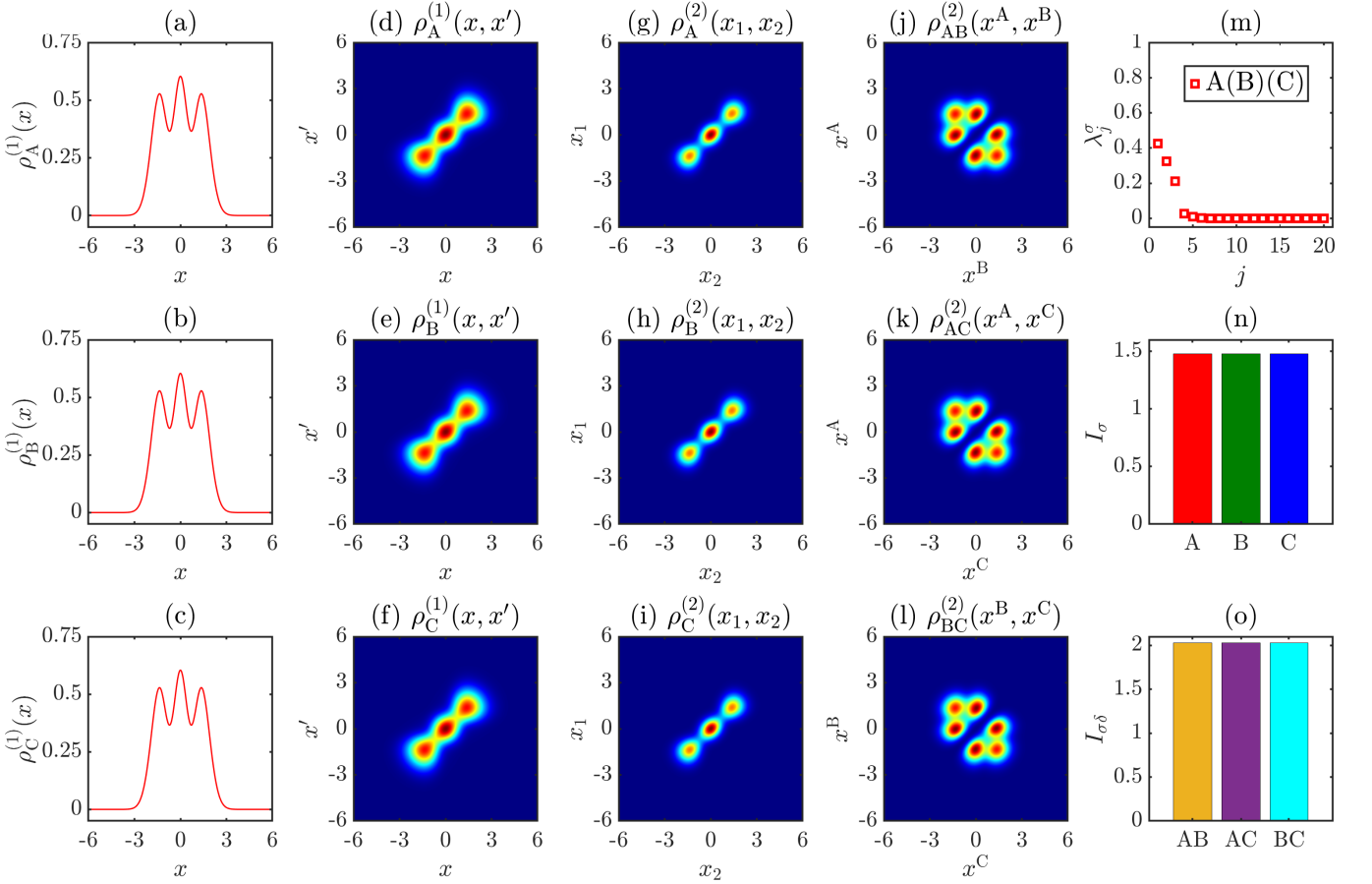


FIG. 6. The ‘Triple Composite Fermionization’ phase ($g_{AB} = g_{BC} = g_{AC} \rightarrow \infty$, and $g_A = g_B = g_C = 0$). (a-c) The one-body density distribution function $\rho_\sigma^{(1)}(x)$. (d-f) The one-body density matrix $\rho_\sigma^{(1)}(x, x')$. (g-i) The intraspecies two-body correlation function $\rho_\sigma^{(2)}(x_1, x_2)$. (j-l) The interspecies two-body correlation function $\rho_{\sigma\delta}^{(2)}(x^\sigma, x^\delta)$. (m) The eigenvalues λ_j^σ of the one-body density matrices. (n) The intraspecies mutual information I_σ . (o) The interspecies mutual information $I_{\sigma\delta}$.

repel each other, this phase resembles some features of composite fermionization introduced for two-component bosonic mixtures [28]. The detailed results for this case are depicted in Fig. 6, and one can immediately see that the quantities of interest are identical for all species due to the symmetries in the coupling strengths. The strongly repulsive interspecies interactions result in a one-body spatial density profiles that has three peaks for each component, with the highest probability of finding a σ -species boson at the center of the trap. By looking at the reduced one-body density matrix (Figs. 6(d-f)) one can see that the probability of a σ -species boson at the position x immediately being measured at the position x' mainly distributes along the diagonal $x = x'$, which indicates the absence of off-diagonal long-range order, which is typical for a fermionized state. Furthermore, the two body correlations functions (see panels (g-i) in Fig. 6) show that two atoms of different species cannot be found at same position since $\rho_{\sigma\delta}^{(2)}(x^\sigma, x^\delta)$ is zero along the diagonal owing to the infinitely repulsive intraspecies interaction. However two atoms of same species can be found at the same place, either at the center of trap or slightly displaced to the left or right (Figs. 6(j-l)). For all three components the OBDM has a number of finite eigenvalues, indicating that neither is totally condensed. Finally, since all interspecies coupling strengths are in the strongly repulsive regime, the species have the same inter- and intraspecies correlations (see Figs. 6(n,o)).

2. Full Fermionization

The case in which all interactions are strongly repulsive corresponds to the corner 8.7 in Fig. 1 and is totally symmetric in all species. It is termed ‘Full Fermionization’ and in Fig. 7 we show the numerical results for this case. Due to the full symmetry between all six bosons, they can be found in any order starting from left to right, which

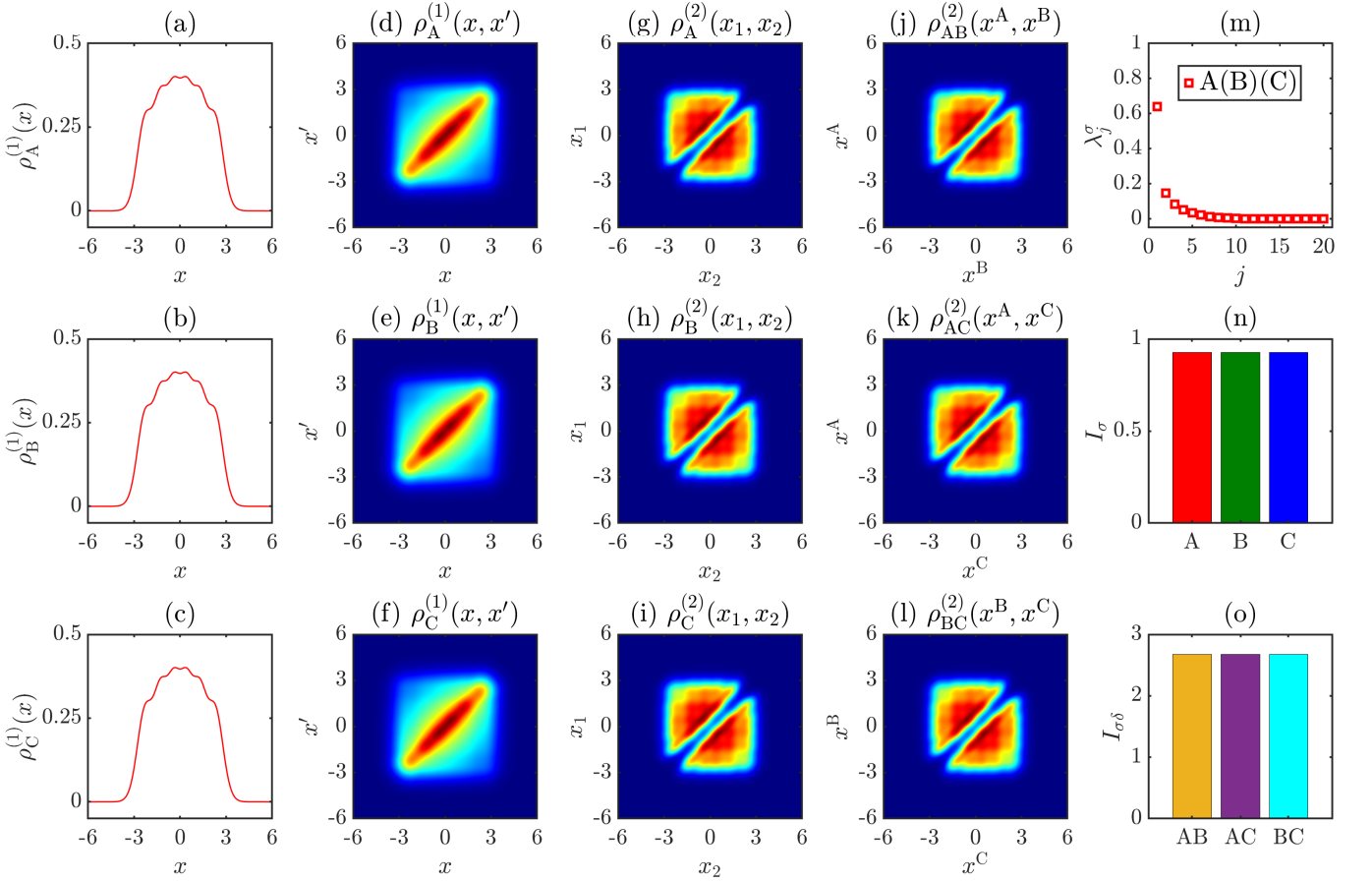


FIG. 7. The ‘Full Fermionization’ phase ($g_A = g_B = g_C = g_{AB} = g_{BC} = g_{AC} \rightarrow \infty$). (a-c) The one-body density distribution function $\rho_\sigma^{(1)}(x)$. (d-f) The one-body density matrix $\rho_\sigma^{(1)}(x, x')$. (g-i) The intraspecies two-body correlation function $\rho_\sigma^{(2)}(x_1, x_2)$. (j-l) The interspecies two-body correlation function $\rho_{\sigma\delta}^{(2)}(x^\sigma, x^\delta)$. (m) The eigenvalues λ_j^σ of the one-body density matrices. (n) The intraspecies mutual information I_σ . (o) The interspecies mutual information $I_{\sigma\delta}$.

results in six peaks in the density profiles depicted in Figs. 7(a-c). It can be understood as a TG gas of six infinitely repulsive bosons which can not be located at the same position as visible in the TBCFs (see Figs. 7(i-o)). In fact the results in this case straightforwardly extend the Full Fermionization case in bosonic binary mixture presented in Refs. [28, 30]. Similar to the ‘‘Triple Composite Fermionization’’ case, each species and each combination possess the same amount of intra- and interspecies correlations as $I_A = I_B = I_C$ and $I_{AB} = I_{AC} = I_{BC}$.

3. Induced Composite Fermionization - Phase Separation

An intriguing case occurs when one of the intraspecies interactions and all three interspecies interactions are large. This case is named as ‘‘Induced Composite Fermionization - Phase Separation’’ and it can appear in three different ways (corners 2.7, 3.7 and 4.7 in Fig. 1). The quantities of interest for corner 2.7, in which $g_A = g_{AB} = g_{BC} = g_{AC} \rightarrow \infty$, $g_B = g_C = 0$, are shown in Fig. 8. One can immediately see from Fig. 8(a) that the infinitely repulsive intraspecies interactions between the A bosons leads to them being separated into two equal parts and localized at the edges. Furthermore, the lack of off-diagonal terms in all OBDMs visible in Figs. 8(d-f), shows the absence of the long-range correlations within each species. These OBDMs show that one can only find bosons of kind A either on the left or right of mostly centered B and C bosons, and consequently $\rho_A^{(1)}(x, x')$ is fragmented with two doubly-degenerate eigenvalues close to $0.5N_A$ as depicted in Fig. 8(m).

The two-body correlations between the two A bosons, Fig. 8(g), show that the particles are anti-bunched, meaning that one will always find one A atom on one side of the trap, and the other A atom on the other side. Meanwhile the atoms of the other two species are localized at the center of the trap and exhibit some features similar to Composite Fermionization phase in binary mixtures [28]. In particular two identical (B or C species) bosons can sit on top each

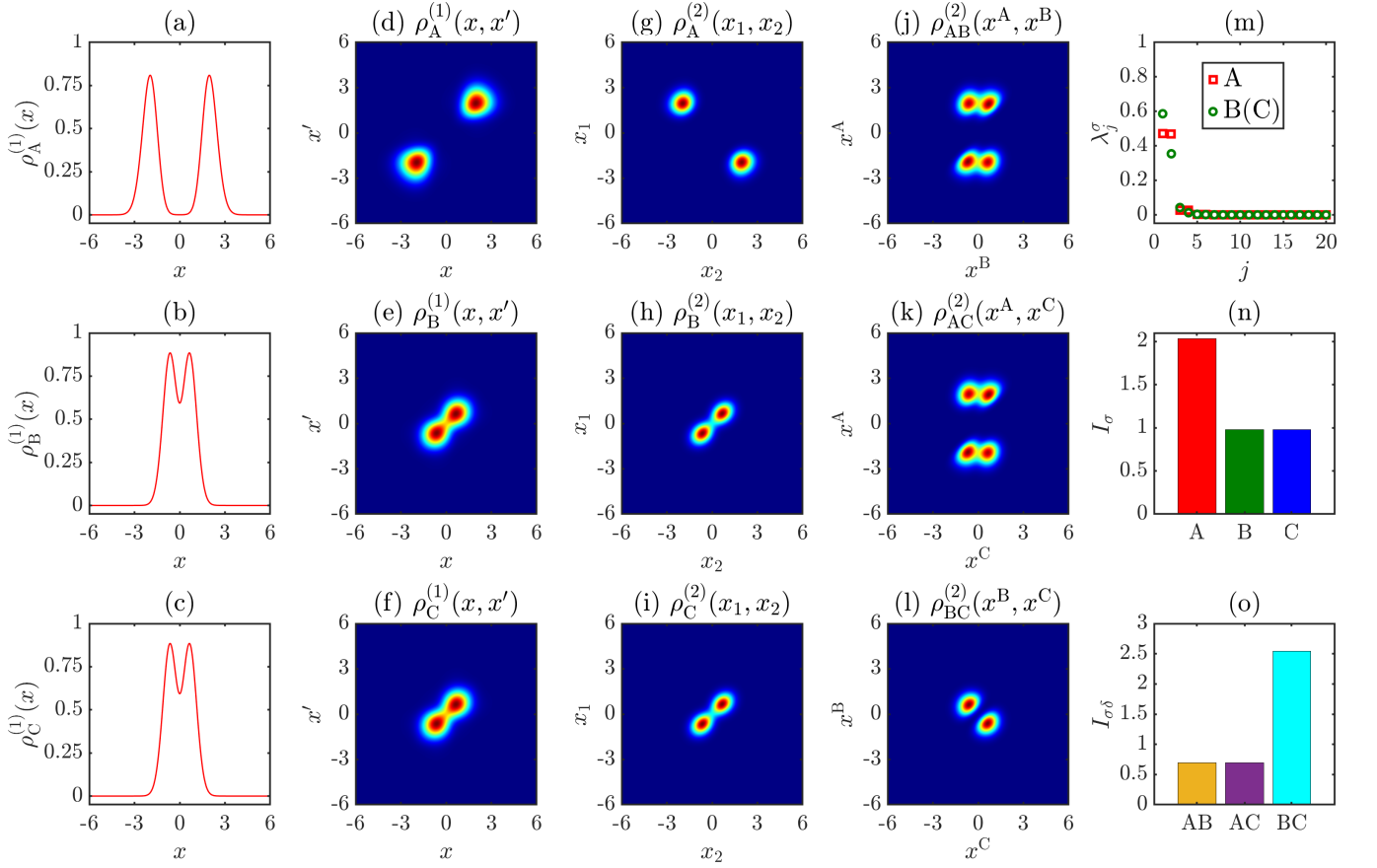


FIG. 8. The ‘Induced Composite Fermionization - Phase Separation’ phase ($g_A = g_{AB} = g_{BC} = g_{AC} \rightarrow \infty$, and $g_B = g_C = 0$). (a-c) The one-body density distribution function $\rho_\sigma^{(1)}(x)$. (d-f) The one-body density matrix $\rho_\sigma^{(1)}(x, x')$. (g-i) The intraspecies two-body correlation function $\rho_\sigma^{(2)}(x_1, x_2)$. (j-l) The interspecies two-body correlation function $\rho_{\sigma\delta}^{(2)}(x^\sigma, x^\delta)$. (m) The eigenvalues λ_j^σ of the one-body density matrices. (n) The intraspecies mutual information I_σ . (o) The interspecies mutual information $I_{\sigma\delta}$.

other, whereas a C boson and a B boson avoid occupying the same place. This is due to the correlations with the A species and the eigenvalues of the OBDM for components B and C show a few finite values, confirming the absence of coherence. The two-body correlation functions for species B and C, Figs. 8(h,i), show that the two bosons of each of these species have a high probability to occupy the same space due to their vanishing intraspecies interactions. However, due to the repulsion between the components, each one is located slightly away from the center of the trap, which can also be clearly seen in the two-body correlations between an A boson and a B (or C) boson in Figs. 8(j,k). Since the interspecies interaction between B and C is large and repulsively, they phase separate with the two B atoms being either on the left or the right of the two C atoms, see Fig. 8(l). Finally, since species A is split, it has a larger amount of intraspecies correlations than species B(C), $I_A > I_B = I_C$, but the components B and C exhibit the highest level of interspecies correlations.

4. Phase Separation

The situation of one component with a strong intraspecies coupling and strong interspecies coupling with the other two components defines the ‘Phase Separation’ case. Due to the symmetry of the interaction strengths, this case is triply degenerated (see the corners 2.6, 3.3, and 4.8) and in the following we present the results of the corner 2.6 whose set of interaction strengths is explicitly give by $g_A = g_{AB} = g_{AC} \rightarrow \infty$ and $g_B = g_C = g_{BC} = 0$. Furthermore, due to the symmetry between the B and the C component, the distribution of the particles obeys the same logic as in the Phase Separation case for Bose-Bose mixture [30]. From the plots in Figs. 9(a-c), one can see that species B and C, whose intraspecies interactions vanish, are confined to the center of the trap and remain coherent with the occupancy of their highest natural orbitals roughly being 0.97. In contrast, species A is split into two equal parts that are located

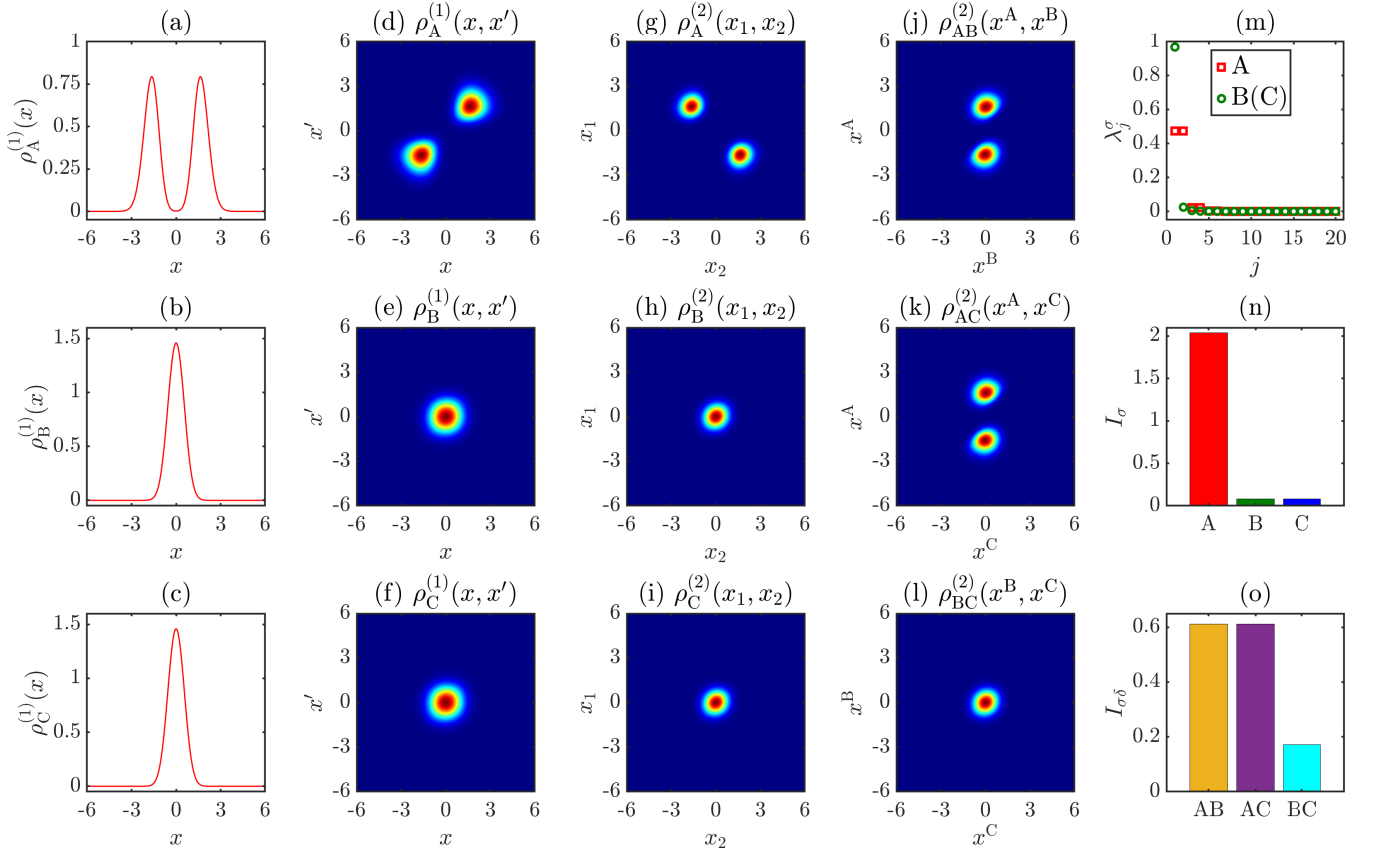


FIG. 9. The ‘Phase Separation’ phase ($g_A = g_{AB} = g_{AC} \rightarrow \infty$ and $g_B = g_C = g_{BC} = 0$). (a-c) The one-body density distribution function $\rho_\sigma^{(1)}(x)$. (d-f) The one-body density matrix $\rho_\sigma^{(1)}(x, x')$. (g-i) The intraspecies two-body correlation function $\rho_\sigma^{(2)}(x_1, x_2)$. (j-l) The interspecies two-body correlation function $\rho_{\sigma\delta}^{(2)}(x^\sigma, x^\delta)$. (m) The eigenvalues λ_j^σ of the one-body density matrices. (n) The intraspecies mutual information I_σ . (o) The interspecies mutual information $I_{\sigma\delta}$.

towards the edges, with zero probability of being found in the center. This results in doubly-degenerated natural orbital occupation numbers of the A species, with both of them close to 0.5. Splitting of the A species due to its strong intraspecies repulsion can be seen in Fig. 9(g), whilst the B and C bosons are located on top each other at the trap center depicted in Figs. 9(h,i,l). These findings are further emphasized in the AB and AC two-body correlation functions, where the likelihood of finding A-type bosons around $x^A = 0$ is fully absent, but two large peaks aligned along $x^{B(C)} = 0$ can be seen in Figs. 9(j,k). Although they do not directly interact with each other, species B and C can be seen to retain a small level of intraspecies correlations induced via the couplings to species A as $I_B = I_C \neq 0$. The infinitely repulsive intraspecies and interspecies interactions with the B and C species leads to the large value of I_A , indicating that species A has very strong intraspecies correlations. In terms of interspecies correlations, the components A and B, and A and C have the same level, which is larger than the one of the components B and C as seen in Fig. 9(o).

5. Correlation-induced Anti-bunching Type II

The case is characterized by all three intraspecies interactions and two interspecies interactions being large is three-fold degenerate. This phase can be found at the corners of the same cube given by 8.3, 8.6 and 8.8 (see Fig. 1). This case shares some similarities with the Correlation-induced Anti-bunching Type I case as can be seen in Fig. 10. In the following we discuss the corner 8.6, for which $g_A = g_B = g_C = g_{AB} = g_{AC} \rightarrow \infty$, and $g_{BC} = 0$. One can see that the two A atoms fragment and that the central B and C clouds form two TG gases according to their OBDM and their intraspecies two-body correlation functions. The two body correlation functions $\rho_{AB}^{(2)}(x^A, x^B)$ and $\rho_{AC}^{(2)}(x^A, x^C)$ are identical and show that the two A bosons are separated, while the B and C bosons spread out due to the strong intraspecies repulsion, but still have large overlap around $x^{B(C)} = 0$ and can be at the same place concurrently.

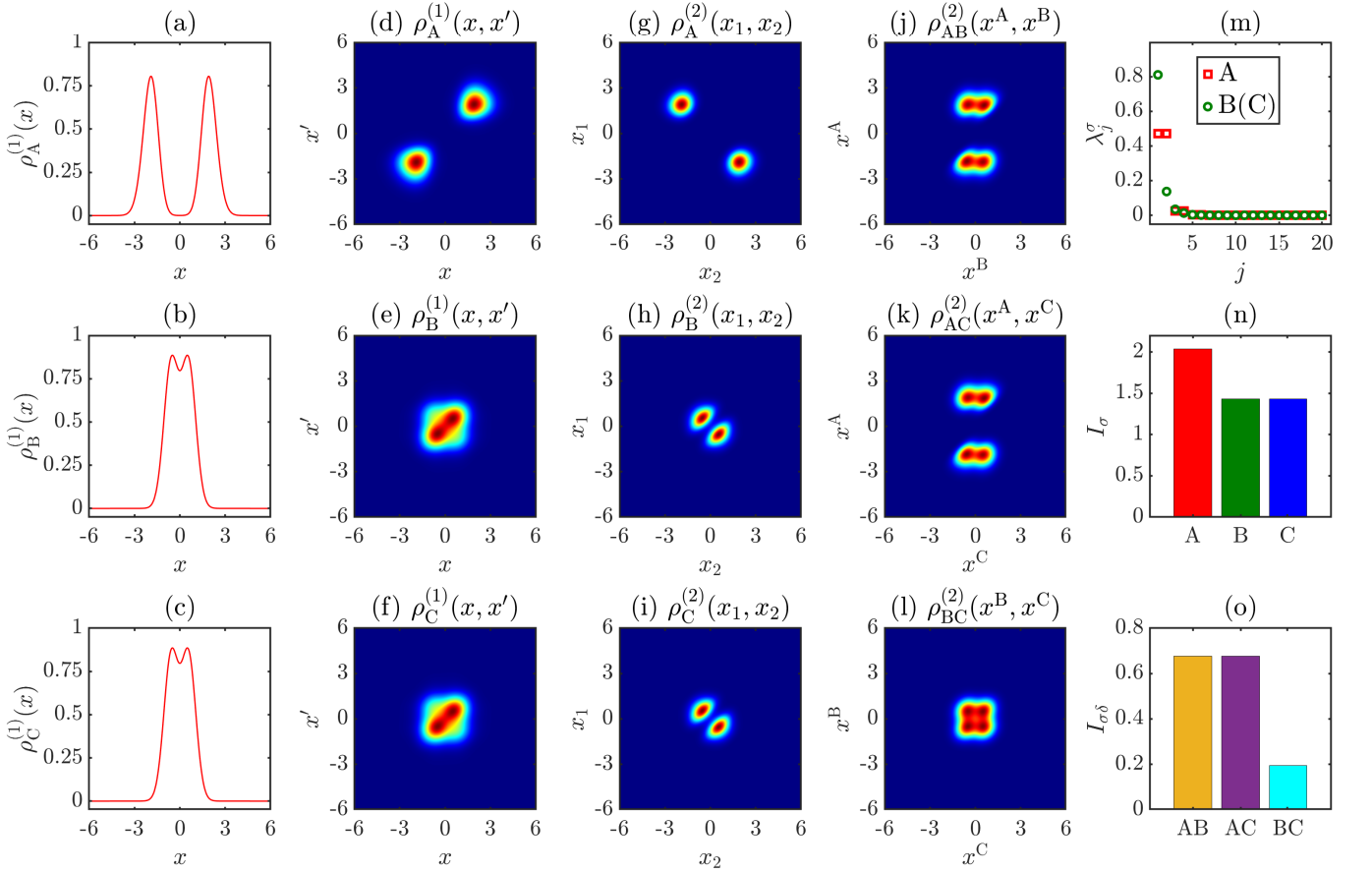


FIG. 10. The ‘Correlation-induced Anti-bunching Type II’ phase ($g_A = g_B = g_C = g_{AB} = g_{AC} \rightarrow \infty$, and $g_{BC} = 0$). (a-c) The one-body density distribution function $\rho_{\sigma}^{(1)}(x)$. (d-f) The one-body density matrix $\rho_{\sigma}^{(1)}(x, x')$. (g-i) The intraspecies two-body correlation function $\rho_{\sigma}^{(2)}(x_1, x_2)$. (j-l) The interspecies two-body correlation function $\rho_{\sigma\delta}^{(2)}(x^{\sigma}, x^{\delta})$. (m) The eigenvalues λ_j^{σ} of the one-body density matrices. (n) The intraspecies mutual information I_{σ} . (o) The interspecies mutual information $I_{\sigma\delta}$.

Furthermore, $\rho_{BC}^{(2)}(x^B, x^C)$ confirms that species B and C are spread around the center of the trap and form two independent squeezed TG gases due to the fact that there is no interspecies interactions. From Fig. 10(n) we can see strong intraspecies correlations in all species, particularly $I_A > I_B = I_C$. As illustrated in Fig. 10(o), the interspecies correlations between species A and B, as well as A and C, are equivalent and exceed those between species B and C, i.e. $I_{AB} = I_{AC} > I_{BC}$.

6. Correlation-induced Bunching Type I

The case in which only two infinitely repulsive interspecies interactions exist is termed ‘Correlation-induced Bunching Type I’. From Table. I one can see that there are three possible realisations corresponding to the corners 1.3, 1.6 and 1.8, and in Fig. 11 we show the realisation corresponding to corner 1.6 with $g_{AB} = g_{AC} \rightarrow \infty$, and $g_A = g_B = g_C = g_{BC} = 0$. This case is dominated by two insights. First, any overlap of component A with either of the other two is energetically costly, however components B and C can overlap. One can see from Figs. 11(a,d) that this leads to component A being split into two parts with its one-body density matrix having two dominant eigenvalues close to 0.5. Additionally, one can see from Fig. 11(g) that $\rho_A^{(2)}(x_1, x_2)$ is concentrated along the diagonal, which means that the two A bosons are bunched at one side of the trap. This is due to the presence of a mediated attractive interaction through the B and C components which acts to bind the A particles together in the absence of intraspecies coupling $g_A = 0$. Second, even though components B and C do not directly interact, they indirectly interact via their respective interactions with component A. This can be confirmed from the fact that their OBDMs possess two large eigenvalues, despite both components showing a Gaussian-like density profile localized about the center of the trap. This is consistent with the narrowing of the one-body correlation functions $\rho_B^{(1)}(x, x')$ and $\rho_C^{(1)}(x, x')$

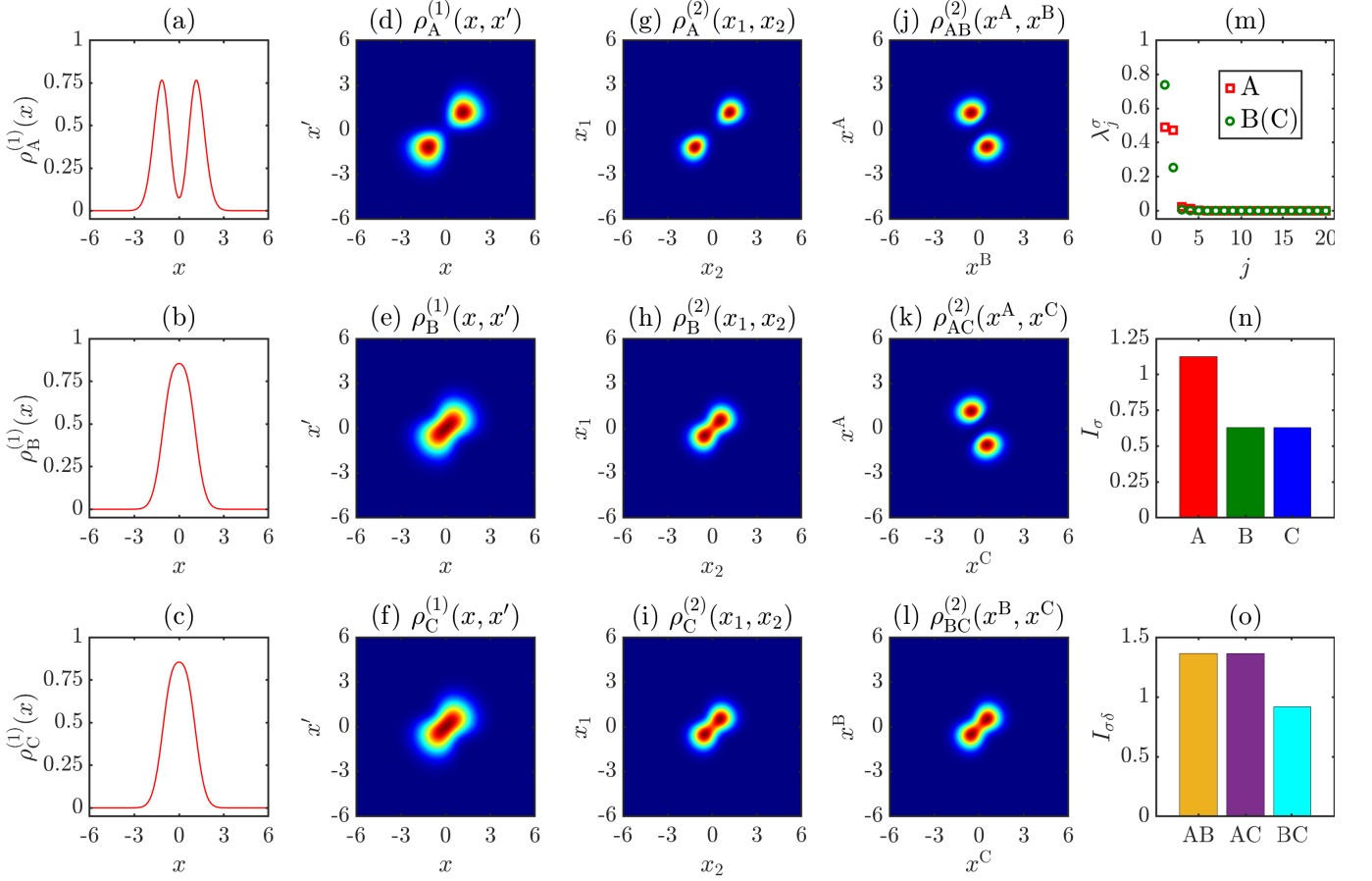


FIG. 11. The ‘Correlation-induced Bunching Type I’ phase ($g_{AB} = g_{AC} \rightarrow \infty$, and $g_A = g_B = g_C = g_{BC} = 0$). (a-c) The one-body density distribution function $\rho_\sigma^{(1)}(x)$. (d-f) The one-body density matrix $\rho_\sigma^{(1)}(x, x')$. (g-i) The intraspecies two-body correlation function $\rho_\sigma^{(2)}(x_1, x_2)$. (j-l) The interspecies two-body correlation function $\rho_{\sigma\delta}^{(2)}(x^\sigma, x^\delta)$. (m) The eigenvalues λ_j^σ of the one-body density matrices. (n) The intraspecies mutual information I_σ . (o) The interspecies mutual information $I_{\sigma\delta}$.

along the off-diagonal $x = -x'$. These mediated interactions are also attractive as seen in the particle bunching along the diagonal of the two-body correlation functions $\rho_B^{(2)}(x_1, x_2)$, $\rho_C^{(2)}(x_1, x_2)$ and $\rho_{BC}^{(2)}(x^B, x^C)$, which are identical due to symmetry between the components. Similar correlation effects are manifested in the two-body correlation functions $\rho_{AB}^{(2)}(x^A, x^B)$ and $\rho_{AC}^{(2)}(x^A, x^C)$ by the peaks being slightly off from $x^{B(C)} = 0$, and all induced correlations can be quantified by the non-zero values of I_A , I_B , I_C and I_{BC} as shown in Figs. 11(n,o).

7. Correlation-induced Bunching Type III

In the final case we discuss two of the intraspecies interactions tend to infinite, and both of these species interact strongly with the remaining one. This phase is triply degenerated and appears at the corners 5.8, 6.3 and 7.6. The results shown in Fig. 12 are for the case in which $g_B = g_C = g_{AB} = g_{AC} \rightarrow \infty$ and $g_A = g_{BC} = 0$. Note that since $g_B = g_C \rightarrow \infty$ and $g_{BC} = 0$, species B and C are symmetric and exhibit the same physics. One can therefore immediately note that species A and B(C) have similar density profiles to the Correlation-induced Bunching Type II phase. More specifically, species B(C) occupies mostly the center of the trap but is extended towards to the edges, starting from position at which $\rho^B(x)$ is exactly equal to its half maximum. The two A-species bosons split and can be found either to the left or to the right of the central B and C cloud as seen from the intraspecies two-body correlations $\rho_{AB}^{(2)}(x^A, x^B)$ and $\rho_{AC}^{(2)}(x^A, x^C)$. Although the two B(C) atoms avoid locating at the same position as $\rho_{B(C)}^{(2)}(x_1, x_2 = x_1) = 0$, one B-type and one C-type boson can be found at same location with high probability at the center of the parabolic trap. Overall, these three species are not totally coherent, with a few natural orbital occupancies

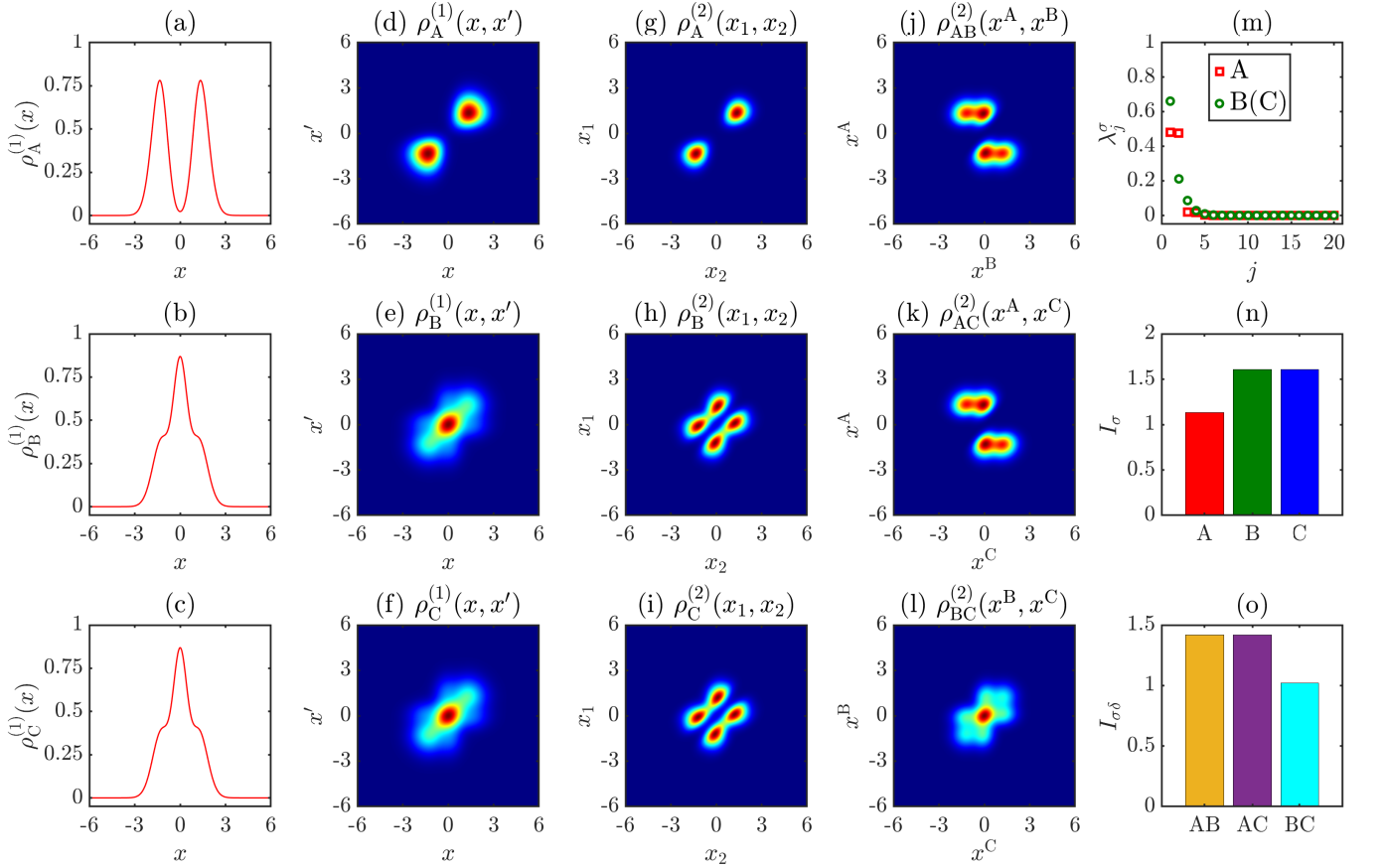


FIG. 12. The ‘Correlation-induced Bunching Type III’ phase ($g_B = g_C = g_{AB} = g_{AC} \rightarrow \infty$ and $g_A = g_{BC} = 0$). (a-c) The one-body density distribution function $\rho_\sigma^{(1)}(x)$. (d-f) The one-body density matrix $\rho_\sigma^{(1)}(x, x')$. (g-i) The intraspecies two-body correlation function $\rho_\sigma^{(2)}(x_1, x_2)$. (j-l) The interspecies two-body correlation function $\rho_{\sigma\delta}^{(2)}(x^\sigma, x^\delta)$. (m) The eigenvalues λ_j^σ of the one-body density matrices. (n) The intraspecies mutual information I_σ . (o) The interspecies mutual information $I_{\sigma\delta}$.

dominantly populated. In comparison with the ‘Correlation-induced Bunching Type II’ phase illustrated in Fig. 4, I_C is substantially enhanced indicating a higher level of intraspecies correlations as $g_C \rightarrow \infty$ and $I_C = I_B > I_A$. Furthermore, it is seen that the level of interspecies correlations in the composite AC increase and is same as the composite AB.

DATA AVAILABILITY

All data that support the findings of this study are included within the article (and any supplementary files).

-
- [1] I. Bloch, J. Dalibard, and S. Nascimbene, Quantum simulations with ultracold quantum gases, *Nat. Phys.* **8**, 267 (2012).
 - [2] T. Karman, M. Tomza, and J. Pérez-Ríos, Ultracold chemistry as a testbed for few-body physics, *Nat. Phys.* , 1 (2024).
 - [3] S. L. Cornish, M. R. Tarbutt, and K. R. Hazzard, Quantum computation and quantum simulation with ultracold molecules, *Nat. Phys.* , 1 (2024).
 - [4] D. DeMille, N. R. Hutzler, A. M. Rey, and T. Zelevinsky, Quantum sensing and metrology for fundamental physics with molecules, *Nature Physics* , 1 (2024).
 - [5] C. J. Pethick and H. Smith, *Bose–Einstein condensation in dilute gases* (Cambridge University Press, 2008).
 - [6] L. Pitaevskii and S. Stringari, *Bose–Einstein condensation and superfluidity*, Vol. 164 (Oxford University Press, 2016).
 - [7] T. Sowinski and M. Á. García-March, One-dimensional mixtures of several ultracold atoms: a review, *Rep. Prog. Phys.* **82**, 104401 (2019).

- [8] S. Mistakidis, A. Volosniev, R. Barfknecht, T. Fogarty, T. Busch, A. Foerster, P. Schmelcher, and N. Zinner, Few-body Bose gases in low dimensions—A laboratory for quantum dynamics, *Phys. Rep.* **1042**, 1 (2023).
- [9] T. Kinoshita, T. Wenger, and D. S. Weiss, Observation of a one-dimensional Tonks-Girardeau gas, *Science* **305**, 1125 (2004).
- [10] T. Kinoshita, T. Wenger, and D. S. Weiss, Local pair correlations in one-dimensional Bose gases, *Phys. Rev. Lett.* **95**, 190406 (2005).
- [11] B. Paredes, A. Widera, V. Murg, O. Mandel, S. Fölling, I. Cirac, G. V. Shlyapnikov, T. W. Hänsch, and I. Bloch, Tonks-Girardeau gas of ultracold atoms in an optical lattice, *Nature* **429**, 277 (2004).
- [12] F. Serwane, G. Zürn, T. Lompe, T. Ottenstein, A. Wenz, and S. Jochim, Deterministic preparation of a tunable few-fermion system, *Science* **332**, 336 (2011).
- [13] A. Wenz, G. Zürn, S. Murmann, I. Brouzos, T. Lompe, and S. Jochim, From few to many: Observing the formation of a Fermi sea one atom at a time, *Science* **342**, 457 (2013).
- [14] G. Zürn, A. Wenz, S. Murmann, A. Bergschneider, T. Lompe, and S. Jochim, Pairing in few-fermion systems with attractive interactions, *Phys. Rev. Lett.* **111**, 175302 (2013).
- [15] G. Zürn, F. Serwane, T. Lompe, A. Wenz, M. G. Ries, J. E. Bohn, and S. Jochim, Fermionization of two distinguishable fermions, *Phys. Rev. Lett.* **108**, 075303 (2012).
- [16] S. Murmann, F. Deuretzbacher, G. Zürn, J. Bjerlin, S. M. Reimann, L. Santos, T. Lompe, and S. Jochim, Antiferromagnetic heisenberg spin chain of a few cold atoms in a one-dimensional trap, *Phys. Rev. Lett.* **115**, 215301 (2015).
- [17] S. Murmann, A. Bergschneider, V. M. Klinkhamer, G. Zürn, T. Lompe, and S. Jochim, Two fermions in a double well: Exploring a fundamental building block of the hubbard model, *Phys. Rev. Lett.* **114**, 080402 (2015).
- [18] A. Bergschneider, V. M. Klinkhamer, J. H. Becher, R. Klemt, L. Palm, G. Zürn, S. Jochim, and P. M. Preiss, Experimental characterization of two-particle entanglement through position and momentum correlations, *Nat. Phys.* **15**, 640 (2019).
- [19] S. Zöllner, H.-D. Meyer, and P. Schmelcher, Correlations in ultracold trapped few-boson systems: Transition from condensation to fermionization, *Phys. Rev. A* **74**, 063611 (2006).
- [20] F. Deuretzbacher, K. Bongs, K. Sengstock, and D. Pfannkuche, Evolution from a Bose-Einstein condensate to a Tonks-Girardeau gas: An exact diagonalization study, *Phys. Rev. A* **75**, 013614 (2007).
- [21] M. Girardeau, Relationship between systems of impenetrable bosons and fermions in one dimension, *J. Math. Phys.* **1**, 516 (1960).
- [22] C. Myatt, E. Burt, R. Ghrist, E. A. Cornell, and C. Wieman, Production of two overlapping Bose-Einstein condensates by sympathetic cooling, *Phys. Rev. Lett.* **78**, 586 (1997).
- [23] M. Cazalilla and A. Ho, Instabilities in binary mixtures of one-dimensional quantum degenerate gases, *Phys. Rev. Lett.* **91**, 150403 (2003).
- [24] O. E. Alon, A. I. Streltsov, and L. S. Cederbaum, Demixing of bosonic mixtures in optical lattices from macroscopic to microscopic scales, *Phys. Rev. Lett.* **97**, 230403 (2006).
- [25] T. Mishra, R. V. Pai, and B. Das, Phase separation in a two-species Bose mixture, *Phys. Rev. A* **76**, 013604 (2007).
- [26] M. A. García-March and T. Busch, Quantum gas mixtures in different correlation regimes, *Phys. Rev. A* **87**, 063633 (2013).
- [27] Y. J. Hao and S. Chen, Ground-state properties of interacting two-component Bose gases in a one-dimensional harmonic trap, *Eur. Phys. J. D* **51**, 261 (2009).
- [28] S. Zöllner, H.-D. Meyer, and P. Schmelcher, Composite fermionization of one-dimensional Bose-Bose mixtures, *Phys. Rev. A* **78**, 013629 (2008).
- [29] M. A. García-March, B. Juliá-Díaz, G. Astrakharchik, T. Busch, J. Boronat, and A. Polls, Sharp crossover from composite fermionization to phase separation in microscopic mixtures of ultracold bosons, *Phys. Rev. A* **88**, 063604 (2013).
- [30] M. A. García-March, B. Juliá-Díaz, G. Astrakharchik, T. Busch, J. Boronat, and A. Polls, Quantum correlations and spatial localization in one-dimensional ultracold bosonic mixtures, *New J. Phys.* **16**, 103004 (2014).
- [31] J. Chen, K. Keiler, G. Xianlong, and P. Schmelcher, Impurity-induced quantum chaos for an ultracold bosonic ensemble in a double well, *Phys. Rev. A* **104**, 033315 (2021).
- [32] T. D. Anh-Tai, M. Mikkelsen, T. Busch, and T. Fogarty, Quantum chaos in interacting Bose-Bose mixtures, *SciPost Phys.* **15**, 048 (2023).
- [33] M. García-March, A. S. Dehkharghani, and N. T. Zinner, Entanglement of an impurity in a few-body one-dimensional ideal Bose system, *J. Phys. B* **49**, 075303 (2016).
- [34] A. S. Dehkharghani, A. G. Volosniev, and N. T. Zinner, Coalescence of two impurities in a trapped one-dimensional Bose gas, *Phys. Rev. Lett.* **121**, 080405 (2018).
- [35] F. Theel, S. I. Mistakidis, K. Keiler, and P. Schmelcher, Counterflow dynamics of two correlated impurities immersed in a bosonic gas, *Phys. Rev. A* **105**, 053314 (2022).
- [36] S. I. Mistakidis, A. G. Volosniev, and P. Schmelcher, Induced correlations between impurities in a one-dimensional quenched Bose gas, *Phys. Rev. Res.* **2**, 023154 (2020).
- [37] S. Mistakidis, G. Katsimiga, G. Koutentakis, and P. Schmelcher, Repulsive fermi polarons and their induced interactions in binary mixtures of ultracold atoms, *New J. Phys.* **21**, 043032 (2019).
- [38] T. D. Anh-Tai, T. Fogarty, S. de María-García, T. Busch, and M. A. García-March, Engineering impurity Bell states through coupling with a quantum bath, *Phys. Rev. Res.* **6**, 043042 (2024).
- [39] L. Chergui, J. Bengtsson, J. Bjerlin, P. Stürmer, G. Kavoulakis, and S. Reimann, Superfluid-droplet crossover in a binary boson mixture on a ring: Exact diagonalization solutions for few-particle systems in one dimension, *Phys. Rev. A* **108**, 023313 (2023).

- [40] S. Mistakidis, T. Mithun, P. Kevrekidis, H. Sadeghpour, and P. Schmelcher, Formation and quench of homonuclear and heteronuclear quantum droplets in one dimension, *Phys. Rev. Res.* **3**, 043128 (2021).
- [41] I. Englezos, P. Schmelcher, and S. Mistakidis, Particle-imbalanced weakly interacting quantum droplets in one dimension, *Phys. Rev. A* **110**, 023324 (2024).
- [42] I. Englezos, S. Mistakidis, and P. Schmelcher, Correlated dynamics of collective droplet excitations in a one-dimensional harmonic trap, *Phys. Rev. A* **107**, 023320 (2023).
- [43] L. Cao, V. Bolsinger, S. Mistakidis, G. Koutentakis, S. Krönke, J. Schurer, and P. Schmelcher, A unified ab initio approach to the correlated quantum dynamics of ultracold fermionic and bosonic mixtures, *J. Chem. Phys.* **147**, <https://doi.org/10.1063/1.4993512> (2017).
- [44] L. Cao, S. Krönke, O. Vendrell, and P. Schmelcher, The multi-layer multi-configuration time-dependent hartree method for bosons: Theory, implementation, and applications, *J. Chem. Phys.* **139**, <https://doi.org/10.1063/1.4821350> (2013).
- [45] S. Krönke, L. Cao, O. Vendrell, and P. Schmelcher, Non-equilibrium quantum dynamics of ultra-cold atomic mixtures: the multi-layer multi-configuration time-dependent hartree method for bosons, *New J. Phys.* **15**, 063018 (2013).
- [46] K. Keiler, S. I. Mistakidis, and P. Schmelcher, Polarons and their induced interactions in highly imbalanced triple mixtures, *Phys. Rev. A* **104**, L031301 (2021).
- [47] F. Theel, S. I. Mistakidis, and P. Schmelcher, Crossover from attractive to repulsive induced interactions and bound states of two distinguishable Bose polarons, *SciPost Phys.* **16**, 023 (2024).
- [48] M. Olshanii, Atomic scattering in the presence of an external confinement and a gas of impenetrable bosons, *Phys. Rev. Lett.* **81**, 938 (1998).
- [49] C. Chin, R. Grimm, P. Julienne, and E. Tiesinga, Feshbach resonances in ultracold gases, *Rev. Mod. Phys.* **82**, 1225 (2010).
- [50] E. Haller, M. J. Mark, R. Hart, J. G. Danzl, L. Reichsöllner, V. Melezhik, P. Schmelcher, and H.-C. Nägerl, Confinement-induced resonances in low-dimensional quantum systems, *Phys. Rev. Lett.* **104**, 153203 (2010).
- [51] M. Girardeau, E. M. Wright, and J. Triscari, Ground-state properties of a one-dimensional system of hard-core bosons in a harmonic trap, *Phys. Rev. A* **63**, 033601 (2001).
- [52] M. D. Girardeau and A. Minguzzi, Soluble models of strongly interacting ultracold gas mixtures in tight waveguides, *Phys. Rev. Lett.* **99**, 230402 (2007).
- [53] T. Busch, B.-G. Englert, K. Rzazewski, and M. Wilkens, Two cold atoms in a harmonic trap, *Found. Phys.* **28**, 549 (1998).
- [54] J. Rotureau, Interaction for the trapped Fermi gas from a unitary transformation of the exact two-body spectrum, *Eur. Phys. J. D* **67**, 1 (2013).
- [55] E. Lindgren, J. Rotureau, C. Forssén, A. G. Volosniev, and N. T. Zinner, Fermionization of two-component few-fermion systems in a one-dimensional harmonic trap, *New J. Phys.* **16**, 063003 (2014).
- [56] A. Dehkharghani, A. Volosniev, J. Lindgren, J. Rotureau, C. Forssén, D. Fedorov, A. Jensen, and N. Zinner, Quantum magnetism in strongly interacting one-dimensional spinor Bose systems, *Sci. Rep.* **5**, 10675 (2015).
- [57] L. Rammelmüller, D. Huber, and A. G. Volosniev, A modular implementation of an effective interaction approach for harmonically trapped fermions in 1D, *SciPost Phys. Codebases*, 012 (2023).
- [58] F. Brauneis, H.-W. Hammer, S. M. Reimann, and A. G. Volosniev, Comparison of renormalized interactions using one-dimensional few-body systems as a testbed, *Phys. Rev. A* **111**, 013303 (2025).
- [59] A. Chrostowski and T. Sowinski, Efficient construction of many-body Fock states having the lowest energies, *Acta Phys. Pol. A* **136**, 566 (2019).
- [60] M. Plodzien, D. Wiater, A. Chrostowski, and T. Sowinski, Numerically exact approach to few-body problems far from a perturbative regime, arXiv preprint arXiv:1803.08387 <https://doi.org/10.48550/arXiv.1803.08387> (2018).
- [61] A. Becker, G. M. Koutentakis, and P. Schmelcher, Synthetic dimension-induced pseudo Jahn-Teller effect in one-dimensional confined fermions, *Phys. Rev. Res.* **6**, 013257 (2024).
- [62] D. Pecak and T. Sowinski, Signatures of unconventional pairing in spin-imbalanced one-dimensional few-fermion systems, *Phys. Rev. Res.* **2**, 012077 (2020).
- [63] A. Rojo-Francàs, F. Isaule, and B. Juliá-Díaz, Direct diagonalization method for a few particles trapped in harmonic potentials, *Phys. Rev. A* **105**, 063326 (2022).
- [64] P. Lydźba and T. Sowiński, Signatures of quantum chaos in low-energy mixtures of few fermions, *Phys. Rev. A* **106**, 013301 (2022).
- [65] A. Rojo-Francàs, F. Isaule, and B. Juliá-Díaz, Few particles with an impurity in a one-dimensional harmonic trap, *Phys. Scr.* **99**, 045408 (2024).
- [66] O. Penrose and L. Onsager, Bose-Einstein condensation and liquid helium, *Phys. Rev.* **104**, 576 (1956).
- [67] P. Torma and K. Sengstock, *Quantum Gas Experiments: Exploring Many-Body States*, Vol. 3 (World Scientific, 2014).
- [68] Y. Guo, H. Yao, S. Ramanjanappa, S. Dhar, M. Horvath, L. Pizzino, T. Giamarchi, M. Landini, and H.-C. Nägerl, Observation of the 2d–1d crossover in strongly interacting ultracold bosons, *Nat. Phys.*, 1 (2024).
- [69] L. Amico, R. Fazio, A. Osterloh, and V. Vedral, Entanglement in many-body systems, *Rev. Mod. Phys.* **80**, 517 (2008).
- [70] D. Murphy, J. McCann, J. Goold, and T. Busch, Boson pairs in a one-dimensional split trap, *Phys. Rev. A* **76**, 053616 (2007).
- [71] V. Coffman, J. Kundu, and W. K. Wootters, Distributed entanglement, *Phys. Rev. A* **61**, 052306 (2000).
- [72] S. Musolino, M. Albert, A. Minguzzi, and P. Vignolo, Symmetry oscillations in strongly interacting one-dimensional mixtures, *Phys. Rev. Lett.* **133**, 183402 (2024).
- [73] R. E. Barfknecht, A. Foerster, and N. T. Zinner, Effects of interaction imbalance in a strongly repulsive one-dimensional Bose gas, *Few-Body Syst.* **59**, 1 (2018).

- [74] L. Yang and X. Cui, Effective spin-chain model for strongly interacting one-dimensional atomic gases with an arbitrary spin, *Phys. Rev. A* **93**, 013617 (2016).
- [75] P. Massignan, J. Levinsen, and M. M. Parish, Magnetism in strongly interacting one-dimensional quantum mixtures, *Phys. Rev. Lett.* **115**, 247202 (2015).
- [76] G. Aupetit-Diallo, G. Pecci, C. Pignol, F. Hébert, A. Minguzzi, M. Albert, and P. Vignolo, Exact solution for SU(2)-symmetry-breaking bosonic mixtures at strong interactions, *Phys. Rev. A* **106**, 033312 (2022).
- [77] D. A. Sivak and G. E. Crooks, Thermodynamic metrics and optimal paths, *Phys. Rev. Lett.* **108**, 190602 (2012).
- [78] M. Tomka, T. Souza, S. Rosenberg, and A. Polkovnikov, Geodesic paths for quantum many-body systems, arXiv preprint arXiv:1606.05890 <https://doi.org/10.48550/arXiv.1606.05890> (2016).